QUANTUM DOT LABELLED ANTIMALARIALS AND INVESTIGATION OF THEIR INTERACTION WITH SYNTHETIC HAEMOZOIN

UNIVERSITÀ DI PARMA

University of Cape Town

Thesis submitted to the

UNIVERSITY OF CAPE TOWN

in fulfilment of the requirements for the degree of

Master of Science IN CHEMISTRY

pursuant to the "BRICS" double degree program

by

Giacomo Ganazzoli

FEBRUARY 2018

SUPERVISOR	**CO-SUPERVISOR**
Professor Timothy Egan	Professor Dominga Rogolino

The copyright of this thesis vests in the author. No quotation from it or information derived from it is to be published without full acknowledgement of the source. The thesis is to be used for private study or non-commercial research purposes only.

Published by the University of Cape Town (UCT) in terms of the non-exclusive license granted to UCT by the author.

University of Cape Town

DECLARATION

Quantum Dot Labelled Antimalarials and Investigation of Their Interaction with Synthetic Haemozoin

I, Giacomo Ganazzoli, declare the following:

1. That the above-titled report is my own work, both in concept and execution, apart from the normal guidance of my supervisors;
2. That in cases where others' work has been cited, this has been acknowledged and referenced;
3. That this work has been submitted at University of Parma in accordance with the "BRICS" double degree program for the degree of Master of Science;
4. That I grant the University of Cape Town free licence to reproduce this work, in whole or in part, for the purpose of research.

I hereby present this report in fulfilment of the requirements for the degree Master of Science in Chemistry pursuant to the "BRICS" double degree program between the University of Cape Town and the University of Parma.

Signed by candidate

February 2018

ACKNOWLEDGEMENTS

I would like to express my deep gratitude to **Professor Timothy Egan** for the opportunity to work in his research group, for his precious guidance during the course of this project and for his assistance in the preparation of this thesis.

I would also like to thank **Professor Dominga Rogolino**, my co-supervisor, for her support and advice during the writing work when I returned back to Italy.

I am very grateful to all the members of **Egan research group** who helped me for the whole period and made this experience unforgettable: **Ana De Sousa**, **Fabrizio L'abbate**, **John Okombo**, **Nicola Dare**, **Roxanne Mohunlal** and also **Jill Combrinck**, **Roxanne Openshaw** and **John Woodland.**

I am also thankful to members of the **Hunter research group** for premising me to perform the synthetic part of my project in their laboratory, especially to **Dr Sophie Rees-Jones** who patiently helped me during this time.

Special thanks to the **Administrative staff of Chemistry Department** and in particular to **Deirdre Brooks** for her assistance with all the bureaucratic documents and her kindness.

External assistance from the **Scientific Imaging Unit in the Department of Chemical Engineering at the University of Cape Town** for the use of their transmission and scanning electron microscopes.

My gratitude is extended to the whole **Chemistry Department of the University of Cape Town** for the great hospitality given and for the nice time spent there

ABSTRACT

Chloroquine (CQ) is a well-known antimalarial drug acting through the inhibition of the formation of haemozoin crystals in the Plasmodium parasite's digestive vacuole within human infected red blood cells. The formation of haemozoin is considered a defence strategy of the parasite in order to decrease the levels of toxic ferriprotoporphyrin (Fe(III)PPIX) present in the DV. Chloroquine is supposed to be adsorbed onto the fastest growing face of the crystal, inhibiting the growth and increasing the amount of toxic Fe(III)PPIX; however, the mechanism of this interaction is still largely unproven.

The study of the interactions of CQ with both Fe(III)PPIX and β-haematin, haemozoin's synthetic crystalline equivalent, can be used to clarify the mechanism of antimalarial action of CQ. In this project a CQ derivative was synthesized and labelled with quantum dots (QDs) in order to exploit their particular fluorescence properties during the investigation of the interaction.

The synthesis of a chloroquine derivative was used in order to insert a primary amino function in the drug suitable for the coupling with QDs. The formation of this derivative (N^1-(2-aminoethyl)-N^4-(7-chloroquinolin-4-yl)-N^1-methylpentane-1,4-diamine) was achieved through a four step reaction. After the extraction of chloroquine as a free base from diphosphate salt, it was desethylated. The insertion of the new group was obtained through a N-alkylation using a Boc protected aldehyde, leading to the formation of the final product by cleaving the Boc group with TFA.

CdSe/ZnS quantum dots with carboxylic acid functionalized ligands (QD-COOHs) were obtained from Cytodiagnostics. Thanks to their dimension, they presented a fluorescence emission peak at 630 nm. During the characterization, the optimal fluorimeter conditions were found: excitation wavelength was set at 400 nm; photo multiplier voltage (PMT) of 1000 V; slow scan speed and slit widths of 10 nm for excitation and 5 nm for emission. Quantum dots were visualized using TEM technique and their dimension was confirmed. Thanks to previous studies carried out in this lab, a 0.01 M HEPES (pH 7.5) buffer was used for all the experiments in order to afford a good solubility of Fe(III)PPIX and a minimal QD-COOH emission quenching.

In order to use QD-COOHs to study the interactions of CQ with Fe(III)PPIX and β-haematin it was necessary to attach the CQ derivative to QD-COOH. The carboxylate ligand coating allows the

formation of covalent bonds, coupling the primary amine-function of chloroquine derivative (CQ-NH_2) and QD-COOH. The reaction was completed using a two-step, one-pot process with 1-ethyl-3-(3-dimethylaminopropyl)carbodiimide (EDC) as a coupling agent.

The product of the reaction, chloroquine derivative-labelled CdSe/ZnS quantum dot (QD-CQ), was characterized, recording the fluorescence emission spectrum with maximum intensity peak at 630 nm. In order to verify the achieved functionalization, SEM with EDS was used to detect the presence of Cl on the nanoparticles surface. TEM was also used to visualise the physical appearance of the QD-CQ. Labelled nanoparticles showed an enhanced tendency to aggregate than QD-COOH. The aggregation caused a decreasing of the fluorescence emission spectrum intensity. Sonication was shown to partially reduce QD-CQ aggregation and other experiments were done by adding a little quantity of different solvents (ethanol, methanol, acetone and 0.01 M HEPES pH 4.2) without significant improvements in enhancing fluorescence intensity.

Fluorescence emission spectra of the interactions of the QD-COOHs with CQ and Fe(III)PPIX were then evaluated for comparison with those of the QD-CQ with both compounds.

The final interaction studied was between β-haematin and the QDs. β-haematin was synthesised in 9.7 M acetate. TEM was used to visualise the interaction between QD-COOHs and QD-CQs with β-haematin. The QD-COOHs showed no selectivity in binding to the β-haematin crystals, whereas the QD-CQs bound primarily to the (001) face. This evidence supports theory that CQ adsorbs to the fastest growing face of β-haematin.

ABBREVIATIONS

Boc	Tert-butyloxycarbonyl
CB	Charge band
CQ	Chloroquine
d-H_2O	Deionized water
DV	Digestive vacuole
DCM	Dichloromethane
E_{att}	Attachment energy
EDC	1-Ethyl-3-(3-dimethylaminopropyl)carbodiimide
EDS	Energy dispersive spectroscopy
Em λ_{max}	Emission wavelength
EtOH	Ethanol
Ex λ_{max}	Excitation wavelength
Fe(III)PPIX	Haem/ferriprotoprphyrin IX
τ	Fluorescence lifetime
FTIR	Fourier transform infrared spectroscopy
Hb	Haemoglobin
HEPES	4-(2-Hydroxyethyl)-1-piperazineethanesulfonic acid
HOMO	Highest occupied molecular orbital
HPLC	High Performance Liquid Chromatography
HZ	Haemozoin
IFE	Inner filter effect

IR-ATR	Infrared attenuated total reflectance spectroscopy
LUMO	Lowest unoccupied molecular orbital
NMR	Nuclear magnetic resonance
PBS	Phosphate-buffered saline
PEG	Poly ethylene glycol
pIFE	Primary inner filter effect
PMT	Photo multiplier voltage
PXRD	Powder X-Ray diffraction
QD	Quantum dot
QD-COOH	Carboxylic acid functionalized CdSe/ZnS quantum dot
CQ-NH_2	Chloroquine derivative bearing primary amine side chain
QD-CQ	Chloroquine labelled CdSe/ZnS quantum dot
RBC	Red blood cell
SEM	Scanning electron microscopy
TEM	Transmission electron microscopy
TFA	Trifluoroacetic acid
THF	Tetrahydrofuran
TLC	Thin layer chromatography
Tris	Tris(hydroxymethyl)aminomethane
UV-Vis	UV-Visible spectroscopy
VB	Valence band

Table of Contents

Chapter 2: Aim and Objectives

Chapter 3: Results and Discussion

Chapter 4: Conclusions and Future Work

Chapter 5: Experimental

CHAPTER 1

Introduction

1.1. Malaria and Haemozoin

Malaria is still one of the most dangerous and infectious diseases all over the world. In 2016, as reported by the World Health Organisation, there were 216 million cases of malaria worldwide resulting in an estimated 445,000 deaths.[1] This disease is widespread especially through the tropical and subtropical regions including the majority of Sub-Saharan Africa, Asia, and Latin America.[2] Approximately 90% of both cases and deaths occurred in Africa: most of them occur in children under 15 years old and about 125 million pregnant women are at risk of infection every year.[3] Although in these last few years, a decrease in malaria's incidence has been recorded, there still is much to do to eradicate this disease. In fact, malaria is curable and preventable but poverty and lack of access to proper treatment are the main causes of its high mortality, especially in rural areas (Figure 1.1).

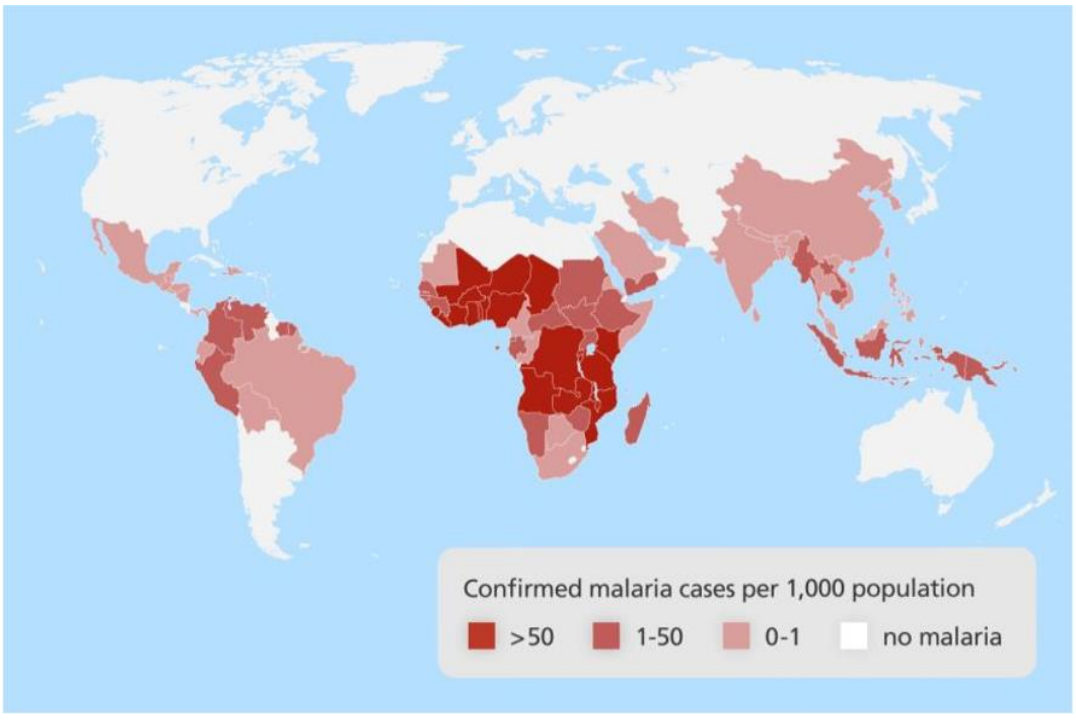

Figure 1.1. Global distribution of malaria cases in 2014.[4]

Malaria is caused by the infection of protozoan parasites belonging to the genus *Plasmodium*. Four species of *Plasmodium* are mainly responsible for infection in humans, namely *P. falciparum, P. malariae*, *P. ovale* and *P. vivax*. Of these, *P. falciparum* is at the origin of most malaria cases, since it is the most virulent and the most prevalent *Plasmodium* species, especially in Africa.[5] Common symptoms of malaria include recurrent fever and headaches. In serious cases, infection can lead to long-term liver and/or neurological damage, coma and death.

The primary hosts and transmission vectors of the malaria parasites are female *Anopheles* mosquitoes. For this reason, the prevalence of the disease varies across the globe according to exposure to the mosquito, with major incidence in tropical and subtropical areas.

1.1.1. Life cycle of *Plasmodium falciparum*

Plasmodium falciparum infection begins with the injection of sporozoites into the bloodstream by an infected female Anopheles mosquito. The sporozoites reach the liver and rapidly invade hepatocytes; they are then involved in a exo-erythrocytic stage leading to maturation to liver schizonts which then rupture, releasing thousands of merozoites into the human blood stream. Merozoites start invading human red blood cells, or erythrocytes, and the erythrocytic stage begins. This stage permits *P. falciparum* to replicate massively inside human organism, generating new merozoites which continue the invasion. During this process a portion of the parasites undergo asexual multiplication into gametocytes. Gametocytes re-enter inside the female *Anopheles* mosquito and begin a new growth cycle within the mosquito vector that will bring the formation of new sporozoites then transmitted to another human (Figure 1.2).

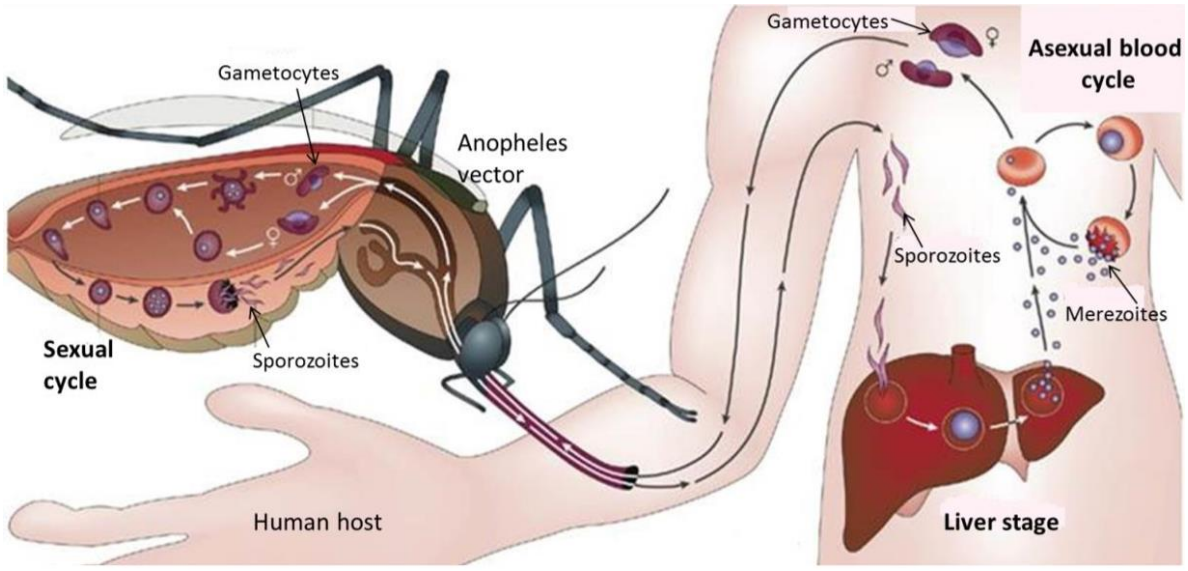

Figure 1.2. Simplified diagram of the Plasmodium life cycle.[6]

1.1.2. Haemoglobin degradation

Living inside the human red blood cells during the erythrocytic stage, the *Plasmodium* parasite is able to use haemoglobin, particularly abundant in these cells, as a nutrient source. In particular, by degrading haemoglobin into peptides in an acidic digestive vacuole, the parasite can provide some amino acids necessary for its subsistence (Figure 1.3.).

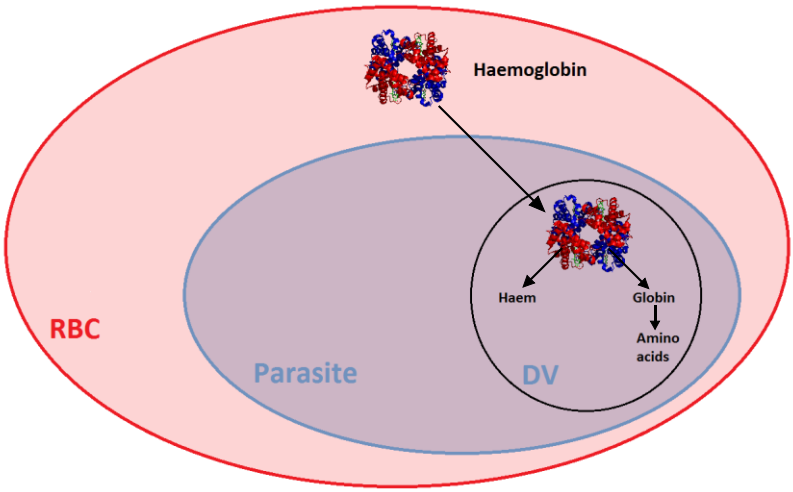

Figure 1.3. Schematic representation of haemoglobin degradation in the digestive vacuole of a parasite in a human host red blood cell.

Haemoglobin is composed by four globular protein subunits, each one comprising a globin chain associated with an iron-containing prosthetic group called haem. During haemoglobin degradation, each haemoglobin molecule releases four haem groups. Once released, haem is rapidly and irreversibly oxidised to its ferric form known as ferriprotoporphyrin IX (Fe(III)PPIX) or haematin when the iron ion is coordinated by a water molecule (Figure 1.4.).

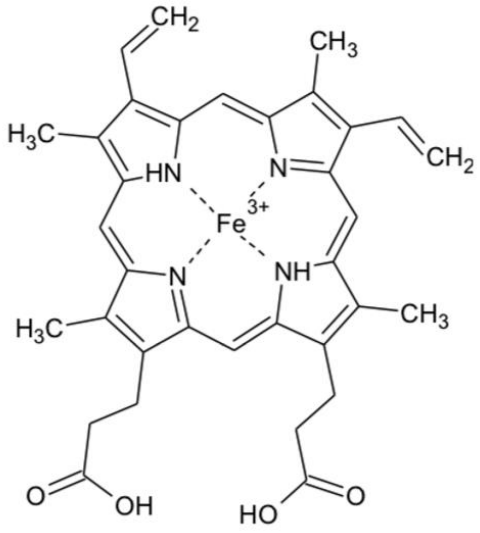

Figure 1.4. Structure of Fe(III)PPIX as product of haemoglobin degradation inside the digestive vacuole of the *Plasmodium* parasite.

1.1.3. Haemozoin formation

Due to its high pro-oxidant activity, Fe(III)PPIX is thought to be highly cytotoxic for the parasite, probably inducing oxidative stress in the organism by reacting with molecular oxygen and producing reactive oxygen species that can destroy the integrity of the cell.[7] In order to get rid of this toxic by-product, Fe(III)PPIX is biocrystallised to an inert, non-toxic, crystalline substance known as haemozoin, within the acidic digestive vacuole.

The crystallization occurs through dimerization during which one carboxylate group of one porphyrin unit coordinates the haem iron(III) of the other and vice versa with subsequent π-stacking of the rings. These cyclic dimers can then interact with each other through hydrogen bonding

interactions between remaining carboxylate groups (Figure 1.5). This detoxification process protects the parasite by packaging Fe(III)PPIX within an insoluble crystalline structure which is not toxic to the parasite.[8]

The synthetic counterpart of haemozoin is called β-haematin and the two species are chemically, spectroscopically and crystallographically identical.[9]

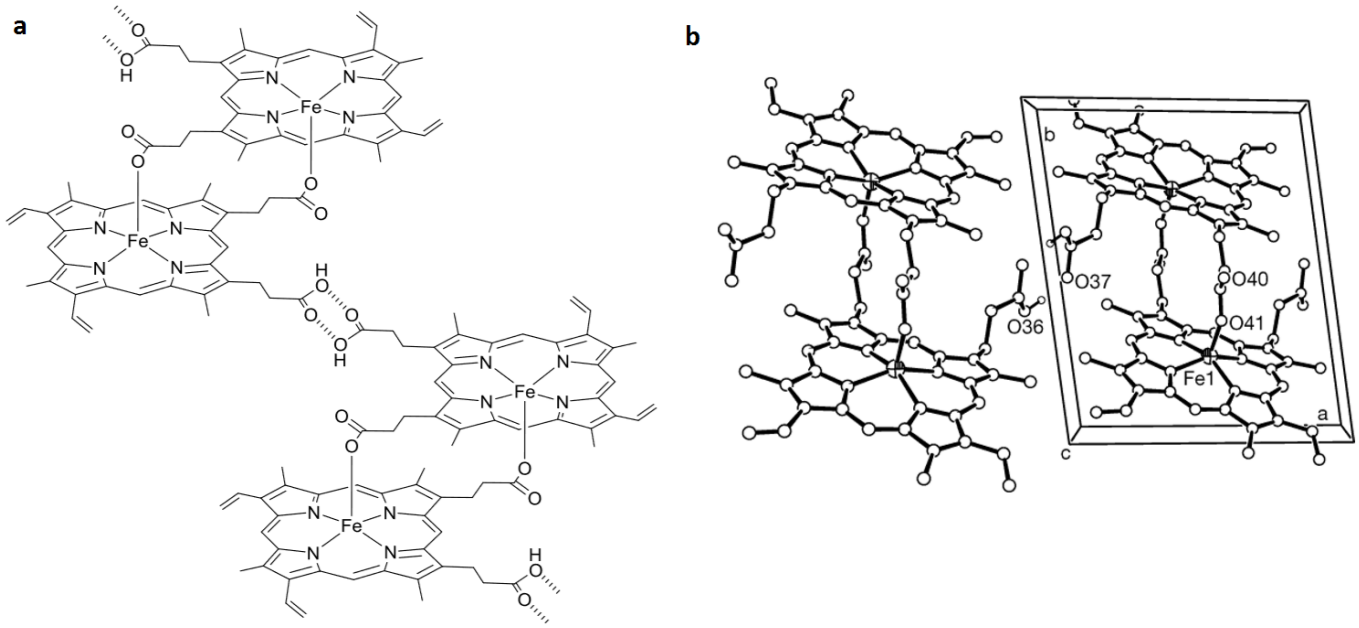

Figure 1.5. Structure of haemozoin (**a**)[10] and crystal structure of its synthetic equivalent β-haematin (**b**)[9].

1.1.4. Inhibition of haemozoin formation

Historically, a substantial number of antimalarial drugs have belonged to the family of quinolines: quinine is their natural progenitor and it is extracted from plants belonging to the genus *Cinchona* (Figure 1.6). Quinoline methanols and 4-aminoquinolines, are believed to target the intraerythrocytic stage of the parasite's life cycle by inhibiting haemozoin formation, leading to a toxic accumulation of Fe(III)PPIX that eventually poisons the parasite.

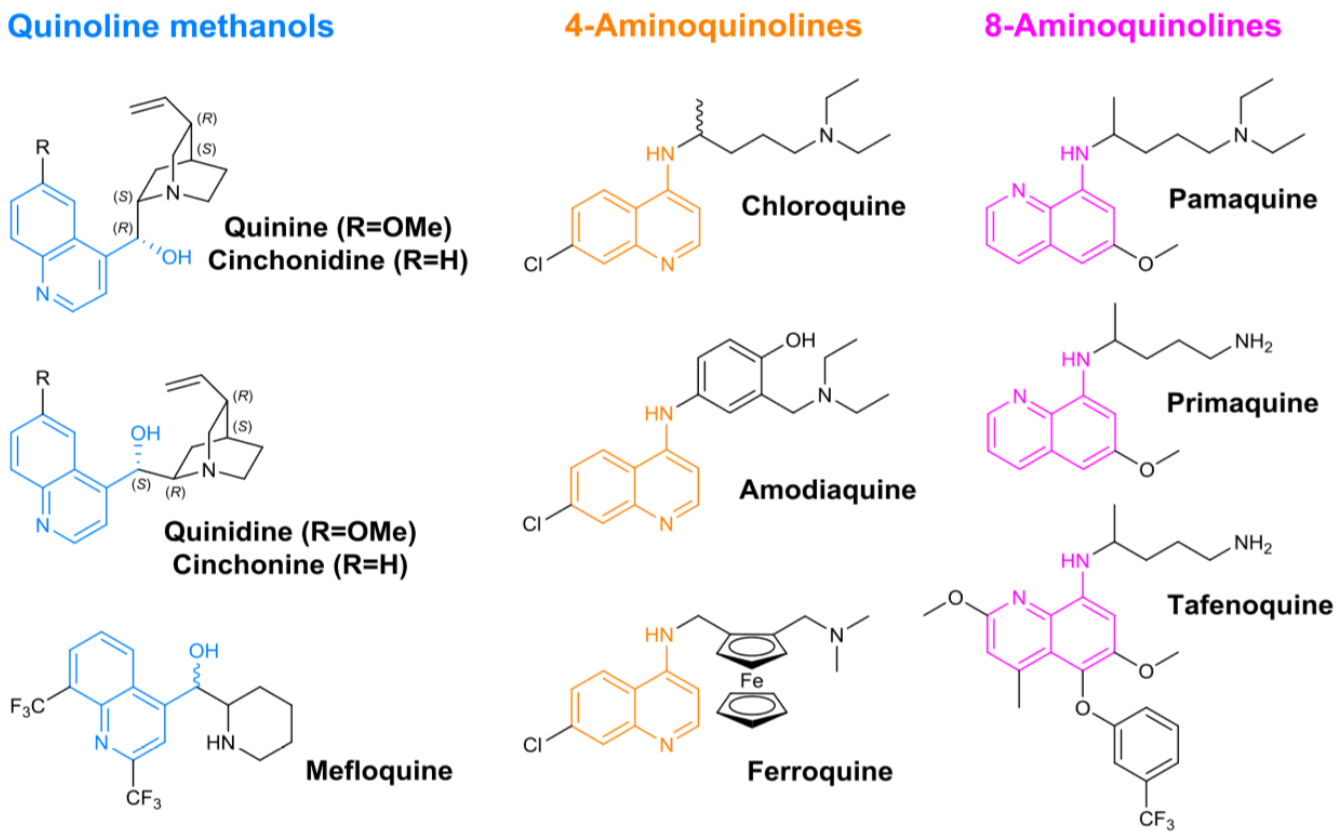

Figure 1.6. Representative compounds of the antimalarial family of quinolines.[10]

Chloroquine (CQ), in particular, has demonstrated to be the most effective and one of the most important antimalarial drugs belonging to the quinoline family. Its mechanism of action is still not completely clear. Current theories explain CQ's antimalarial activity through the inhibition of the formation of haemozoin crystal, permitting an accumulation of toxic free haem inside the parasite causing its death.

The inhibition process could pass through the formation of a Fe(III)PPIX-drug complex where the CQ π-stacks with the Fe(III)PPIX porphyrin ring.[11]

This first proposed mechanism of inhibition by quinoline antimalarials concerns drug-Fe(III)PPIX complex formation. These antimalarials have been suggested to bind Fe(III)PPIX in a form that no longer allows its incorporation into haemozoin, probably by increasing the solubility of the metalloporphyrin. Additionally, these complexes cause deleterious effects on *P. falciparum*. The complex between chloroquine and Fe(III)PPIX enhances the lytic effects on cells that have been observed with Fe(III)PPIX alone.[11,12] Quinine, quinidine and chloroquine all form stable complexes with Fe(III)PPIX in the solution phase, lending support to this hypothesis.

Recent studies, carried out by Combrinck et al. [13,14], have provided a direct evidence of haemozoin inhibition with increased free haem in the parasite.

To examine the effects of CQ on the detoxification process of haem in the malaria parasite, a cell fractionation technique and measurement of Fe(III)PPIX were used. The exposure of the parasite to chloroquine has been shown to cause a dose-dependent decrease in haemozoin and concomitant increase in toxic “free” haem in cultured *Plasmodium falciparum* that is directly correlated with parasite survival. By inhibiting haemozoin formation, chloroquine provokes a correlated increase in toxic free haem which is no longer available for binding crystal surfaces. The curve representing the percentage of “free” Fe(III)PPIX was found to cross the parasite survival curve at approximately the IC_{50} of chloroquine (Figure 1.7).

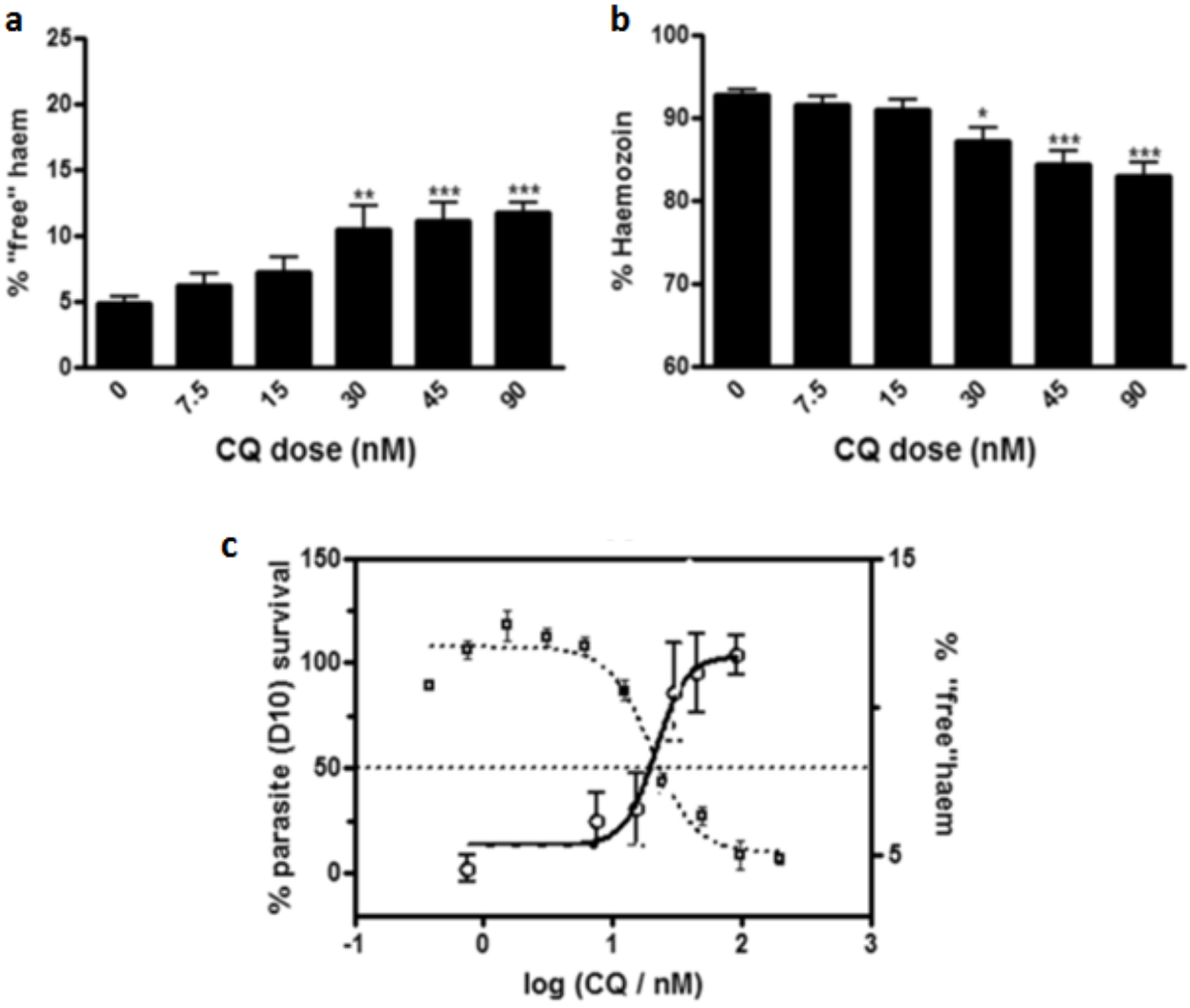

Figure 1.7. Diagrams showing (**a**) the increase of free haem at rising concentration of CQ, (**b**) the correlated decrease of haemozoin and (**c**) decrease in parasite survival.[14]

Transmission electron microscopy techniques have further shown that haem is redistributed from the parasite digestive vacuole to the cytoplasm. In particular, a dramatic increase in cytoplasmic iron concentration could be seen at the trophozoite stage in a region of the malaria parasite that may correspond to the endoplasmic reticulum.

TEM studies have also evinced the presence of a multitude of small crystallites with discernible interfaces between them (grain boundaries) which could be seen at high magnification, demonstrating directly that CQ disrupts the process of haemozoin crystallization in the parasite.

These studies finally provide direct evidence in support of the haemozoin inhibition hypothesis for the mechanism of action of CQ with a resulting dose-dependent build-up of "free" haem in a manner closely matching parasite survival and show that other quinoline and related antimalarials inhibit cellular haemozoin formation.

An alternative theory proposes that the drug adsorbs onto the fastest-growing face of β-haematin crystals, "capping" it and blocking the crystal growth.

This theory is supported by different works of Leiserowitz et al. in which the interaction between different quinoline antimalarials and haemozoin, or β-haematin, crystals has been investigated.

In particular, in many of them they focused on the study of a noncovalent binding site for the quinoline drug family at the end face of the fastest-growing direction of β-haematin crystals. [15,16,17]
This adsorption mechanism has been examined in terms of crystal growth inhibition after the incubation of haemozoin crystals and its analogues with various quinolines. Electron microscope autoradiography studies showed a tendency of quinoline antimalarials in accumulating on the fastest-growing {001} crystal faces of β-haematin. These faces, thanks to the highly negative attachment energy (E_{att} -101.5 kcal/mol), were proposed as the most favourable binding site for quinoline antimalarials. This is due to the pronounced {001} crystal surface corrugation and the presence in the grooves, along the a-axis, of flexible propionic acid groups likely involved in hydrogen bonds between the carboxylic functionalities of neighbouring molecules along the a-c-direction, in addition to vinyl and methyl groups, as well as aromatic surfaces.

In the proposed model, the quinoline aromatic ring is intercalated between porphyrin rings within a crevice at the corrugated {001} surface, to which it is further anchored by a salt bridge between the protonated exocyclic amine and a surface-exposed carboxylate group, in addition to other polar interactions such as, for chloroquine, a CCl···H_3C and a weak (aromatic)N···HC)C(vinyl) hydrogen bond. In chloroquine, the exocyclic amine chain should be sufficiently long and flexible to ensure optimal binding of the distant amine to the host acid group, allow appropriate intercalation of the quinoline, and permit the polar interactions alluded to above (Figure 1.8).[15]

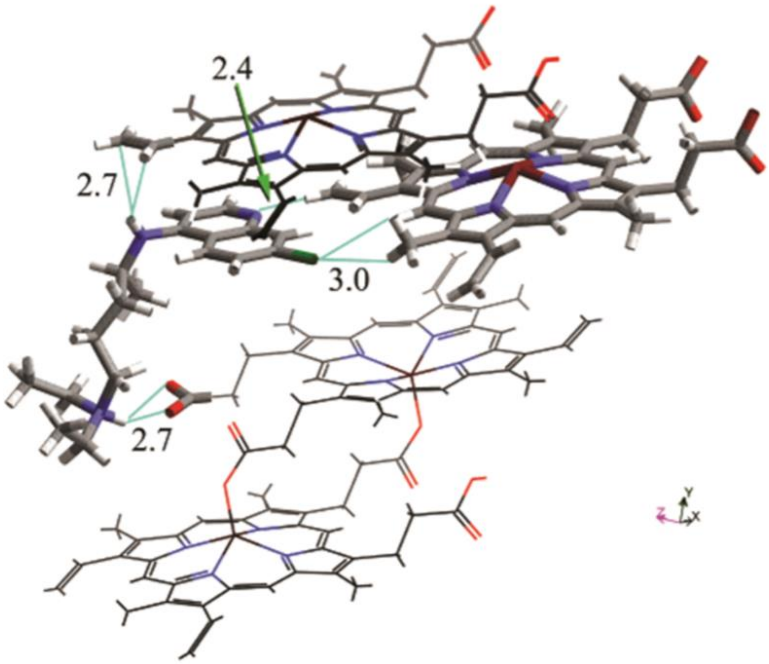

Figure 1.8. Chloroquine bound to the (001) β-haematin crystal highlighting energetically favourable interactions. The distances are between highlighted atoms.[15]

A quinoline such as chloroquine may also bind to the (100) face via the (quinoline) amine···(β-haematin) propionic acid salt bridge, the acid moiety exposed at the crystal surface being sufficiently flexible to adopt an appropriate conformation. By taking advantage of the length of the exocyclic chain, the quinoline ring of chloroquine may also form a "T" type contact with the methyl and vinyl C-H substituents of the haem rings (Figure 1.9).[16]

Also Olafson et al. have directly imaged inhibition of β-haematin crystal growth by chloroquine using time-resolved in situ atomic-force microscopy.[18]

They have observed that the addition of chloroquine to haematin growth solutions leads to slower step growth through the absorption of the drug and blocking the step propagation with a particular specificity for flat {100} surfaces.

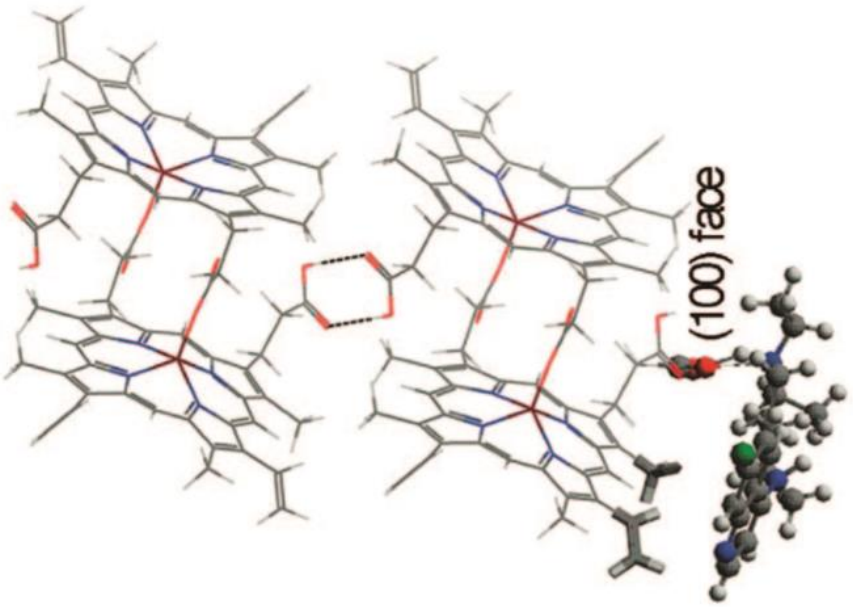

Figure 1.9. Intermolecular contacts between chloroquine and β-haematin at the (100) crystal surface.[16]

They observed also that β-haematin crystals grown in the presence of chloroquine displayed a symmetric tapering at both ends of the needle, resulting in a spine formation of thinner and thinner cross-section. This phenomenon is thought to be a direct effect of inhibition of growth along the c-axis by adsorption of the quinoline additive on the {001} or {011} faces.[16, 17] Analysis using synchrotron PXRD of pure and affected β-haematin, grown in the absence and the presence of quinine and chloroquine, supported the model of quinoline binding to the {001}, {011}, and {100} faces of haemozoin, leading to inhibition of crystal nucleation and growth. During this process, a quinoline molecule may also bind to a β-haematin molecular dimer before the latter is adsorbed on a crystal surface, which has a kinetic disadvantage that the complex must "locate" the appropriate face, say (001) or (001*) on the opposite side of the crystal, onto which to adsorb, depending upon to which of the two carboxyl groups of a β-haematin molecular dimer the drug is bound. Naturally, if both carboxyl groups are bound to quinoline, such a complex cannot be stereoselectively adsorbed onto the crystal surface and so will be ineffective as an inhibitor.[16]

In order to attempt to prove the occurred absorption of quinoline antimalarials on β-haematin crystal surface, different techniques have been proposed to compare results from affected and

unaffected haematin crystals.[17] Synchrotron PXRD studies highlighted that the quinoline additives induce a reduction in the crystal domain size along the c-axis and coherent grazing X-ray diffraction experiments suggested that the β-haematin crystals grown in the presence of the additives were smaller and less structurally stable than the pure form. The IR-ATR and Raman spectral results showed that β-haematin crystals grown in the presence of the quinoline drugs present molecular based differences from pure β-haematin in particular regarding the propionate groups. The results suggest modification of surface and bulk propionic acid linkages and aggregation perturbation within the affected crystal, albeit minor, presumably arising from host molecular rearrangement in the environment of the bulk sites poisoned by occluded quinoline. These proposed changes are consistent with the interpretation of morphological modification, the X-ray diffraction results, and the model computations of surface binding of quinoline antimalarials to the {001} face of β-haematin.[15]

The study of these processes inside the cell is quite difficult. Therefore, in vitro studies are necessary to highlight the mechanism at the basis of the interaction between Fe(III)PPIX, β-haematin and antimalarials. This is why quantum dots (QDs) and their unique fluorescence properties and applications are proposed as a potentially useful tool to improve understanding of such interactions, with a particular focus on CQ.

1.2. Fluorescence Spectroscopy

Fluorescence spectroscopy can be a powerful technique for many possible applications in chemistry, biochemistry and medicine due to its capability in providing highly sensitive, fast, reliable and reproducible detection. In particular, in the case of a fluorescent analyte, fluorescence spectroscopy can provide a direct observation of the species using a fluorimeter operating at appropriate excitation and observation wavelengths.

1.2.1. General principles of fluorescence spectroscopy

Fluorescence is the emission of light at a certain wavelength after a substance called a fluorophore has been excited by an absorption of energy. In the first part of the process, the excitation, the fluorophore absorbs energy and one of its electrons passes from its electronic ground state (S_0) to a singlet excited state (S_1, S_2, ...). The electron, now in the electronic excited state, rapidly relaxes to the lowest vibrational level of the lowest singlet excited state (S_1). This process generally occurs through vibrational and thermal release of energy, called internal conversion. As said the process is very fast due to the proximity in terms of energy of different levels (lifetime of about 10^{-12} seconds). Once the system has reached the S_1 level, different competing pathways can be followed by the molecule to return to its electronic ground state. Energy can be released through a non-radiative relaxation process and dissipated as heat (vibrations); alternatively, the system can release spontaneously the excitation energy in form of electromagnetic radiation (photons) with a specific wavelength corresponding in energy to the gap S_1-S_0 (generally the energy gaps between electronic levels belong to the UV-visible part of the light spectrum). This process is known as fluorescence and typical fluorescence lifetimes (τ) are around 10^{-9} seconds. The molecule could also relax via conversion to a triplet state (T_1) from which it can reach the ground state by non-radiative relaxation or by emitting a photon. Transitions between excited triplet state to a singlet ground state are spin-forbidden and much less probable (lower rate constant). This means longer excited state lifetimes that can go from 10^{-3} seconds to even minutes. These principles are described in Figure 1.10 by a Jablonski diagram.

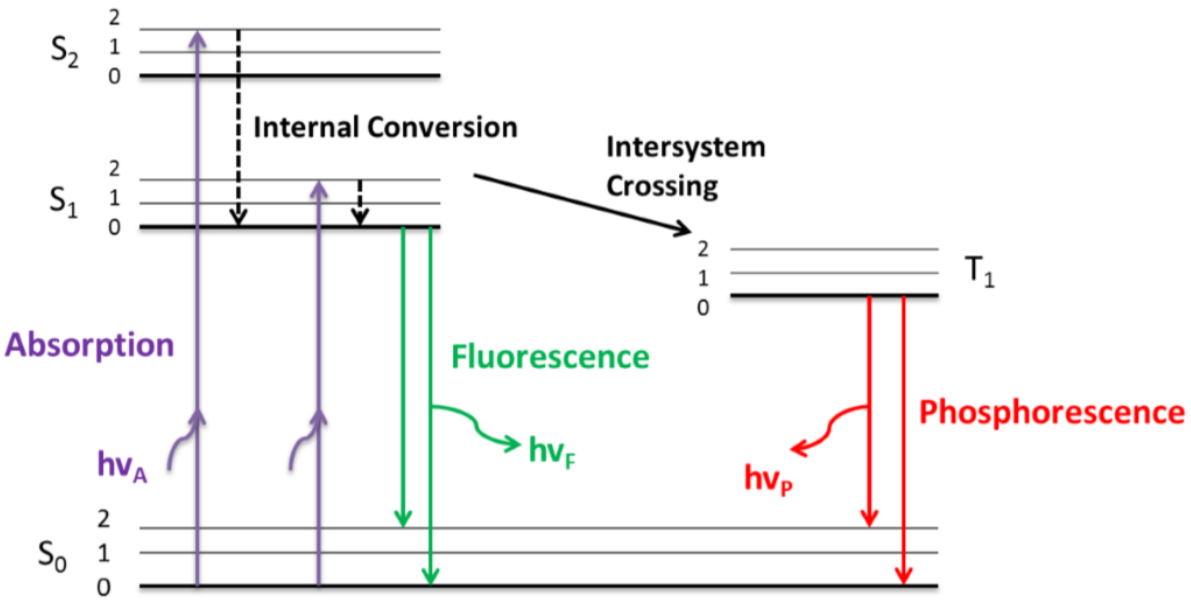

Figure 1.10. Simplified Jablonski diagram depicting singlet and triplet energy states with vibrational energy levels within each state. Absorption or emission of a photon is represented as hv and resultant fluorescence or phosphorescence designated by the green (S_1 to S_0) and red (T_1 to S_0) paths respectively.[19]

The efficiency of the fluorescence process is given by the fluorescence quantum yield (ϕ) defined as the ratio of the number of photons emitted to the number of photons absorbed.

$$\Phi = \frac{number\ of\ emitted\ photons}{number\ of\ absorbed\ photons}$$

Generally, only a little part of the energy absorbed is then re-emitted as fluorescence owing to the other possible routes of relaxation and energy conversion such as decomposition, heat loss or re-emission. There are also a variety of other chemical and experimental factors which are beyond the scope of this report, but an important issue relevant to this project will be discussed further, i.e. the fluorescence quenching process.

1.2.2. Quenching of fluorescence

Fluorescence quenching refers to any process which provokes a decrease in fluorescence intensity. Many intermolecular processes, in which the fluorophore interacts with a quencher, can cause quenching such as excited state reactions, energy transfer, complex-formation (static) and collisional (dynamic) quenching. The two main types of quenching in which we are interested for this project are collisional and static quenching.

Collisional, or dynamic, quenching is observed when, during the fluorophore excited state lifetime (τ), the fluorophore in its excited state comes into contact with the quencher which diffuses through the solution. As a result, the fluorophore returns to its ground state without emitting any radiation and the two molecules remain chemically unaltered after the collision.

For static quenching the contact between fluorophore and quencher generates a non-fluorescent complex, provoking a decrease in fluorescence intensity. Quenching mechanisms differ greatly depending on the compounds and electronic states involved, therefore the focus in this work will be specifically on quantum dots (QDs) and their interactions with Fe(III)PPIX and chloroquine.

In particular, quenching processes can be analysed by measuring the ratio between the observed fluorescence in absence and presence of the quencher. By plotting the obtained value against the concentration of the quencher different types of curves can be observed. In case of pure collisional quenching, a linear trend can be observed, as described by the Stern-Volmer equation:

$$\frac{I_0}{I} = 1 + K_{SV}[\mathrm{Q}] = 1 + k_q \tau_0 [\mathrm{Q}]$$

where K_{SV} is the Stern–Volmer quenching constant, k_q is the bimolecular quenching constant, τ_0 is the lifetime in the absence of quencher, and [Q] is the quencher concentration.

In the case of pure static quenching, again a linear trend is observed according to the equation:

$$\frac{I_0}{I} = 1 + K_a[\mathrm{Q}] \qquad\qquad K_a = \frac{[FQ]}{[F][Q]}$$

where K_a is the fluorophore-quencher association constant, [FQ] is the concentration of the complex, [F] is the concentration of the uncomplexed fluorophore, and [Q] is the concentration of quencher.

When both dynamic and static quenching occur in the system, data are fitted by a parabolic line curving upwards:

$$\frac{I_0}{I} = (1 + K_{SV}[\mathrm{Q}])(\,1 + K_a[\mathrm{Q}]) = 1 + (K_{SV} + K_a)[Q] + K_{SV}K_a[Q]^2$$

Actually, this analysis is not enough to recognize uniquely the type of quenching, especially when a linear trend is observed. In order to distinguish between dynamic and static quenching it is possible to measure the fluorescence excited state lifetime (τ) of the fluorophore in presence of the quencher using time-resolved fluorescence spectroscopy. In fact, in case of collisional dynamic quenching, τ decreases by increasing the quencher concentration. In case of static quenching, τ of the sample does not change by increasing quencher concentration because the reduction of fluorescence intensity is due to the formation of a non-fluorescent complex, reducing the number of fluorophores which can emit.[19]

1.3. Quantum Dots

Quantum dots (QDs) are very small semiconductor particles, whose size is in the range of nanometres (10^{-9} m). Due to their nano-dimensions, they present peculiar optical and electronic properties, different from those of larger particles. These properties, such as absorption and emission wavelength, can be finely tuned by changing the dots' size, shape and material. The peculiar electronic and optical behaviour arises because in QDs the motion of conduction band electrons, valence band holes, or excitons (bound pairs of conduction band electrons and valence band holes) are confined in all three spatial directions. This confinement can be due to electrostatic potentials (generated by external electrodes, doping, strain, impurities), the presence of an

interface between different semiconductor materials (e.g. in core-shell nanocrystal systems), the presence of the semiconductor surface (e.g. semiconductor nanocrystal), or a combination of these.

1.3.1. QDs *versus* organic fluorophores

In fluorescence spectroscopy, organic fluorophores have been widely used during past years to label target molecules, such as biomolecules, to study their nature and behaviour. Unfortunately, the use of organic fluorophores presents many drawbacks; in particular, many organic dyes and protein-based fluorophores suffer from chemical and photophysical liabilities including pH dependence, self-quenching at high concentrations, susceptibility to photo-bleaching, short-term aqueous stability, narrow absorption windows with very broad emission spectra and short excited state fluorescent lifetimes.[20]

In the last 20 years the use of QDs has emerged as a potential solution to many of the issues associated with organic dye and protein-based fluorophores. Their advantage is primarily due to their discrete electronic energy levels and electronic properties arising from this.[21] Quantum dots (QDs) possess many properties making them extremely powerful, including high quantum yields, broad absorption due to large extinction coefficients (10 to 100 times higher than typical organic fluorophores), narrow fluorescence spectra, long fluorescent lifetimes, excellent photostability and tuneable emissions. Moreover, high surface-to-volume ratio further renders QDs ideal for functionalization to obtain good biocompatibility and sensitivity. On the other hand, the major problems in working with QDs are related to their relatively high cost, potential blinking properly termed fluorescence intermittency, toxicity and the occurrence of the inner filter effect (IFE). In addition, QD's are subject to aggregation which can disturb fluorescence measurements by reducing fluorescence intensity.[21, 22]

1.3.2. CdSe/ZnS QDs

In this study cadmium selenide (CdSe) core quantum dots covered by a zinc sulphide (ZnS) shell, functionalised with carboxylic acid ligands on the surface of the QD have been used (Figure 1.11). The ZnS coating contributes to higher quantum yields and greater stability in solutions, decreasing the likelihood of blinking.[23]

CdSe/ZnS quantum dots were purchased by Cytodiagnostics.[24] Their precise shape and dimension, meticulously controlled during synthesis[25], results in a fluorescence emission wavelength of 630 nm.

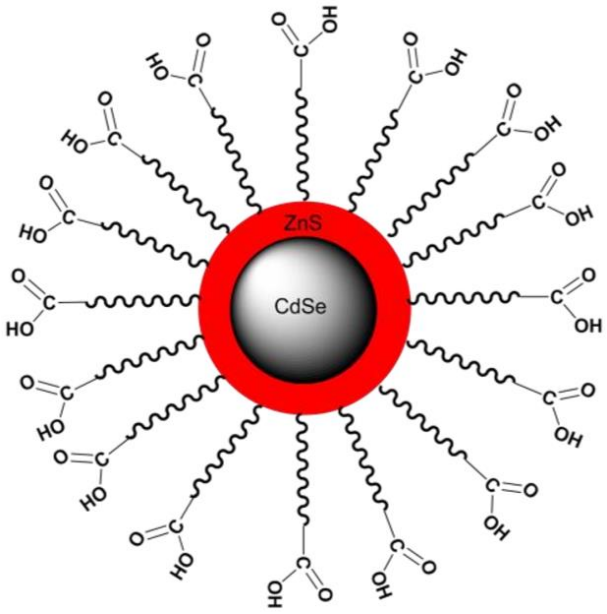

Figure 1.11. Schematic representation of CdSe/ZnS quantum dots functionalised with carboxylic groups on the surface.

1.3.3. Chemical interactions of QDs

Thanks to quantum dots particular fluorescence properties it is possible to exploit fluorescence quenching processes to study the interaction between QDs and a quencher. For this project, different interactions will be investigated exploiting QDs fluorescence properties.

Fe(III)PPIX is known for its ability to act as a quencher for quantum dots. The quenching of fluorescence of QDs by Fe(III)PPIX is proposed to predominantly occur through a static charge transfer mechanism (section 1.2.2). The iron in haem has an oxidation state of 3+, therefore it can act as an electron acceptor as its LUMO is close in energy to the that of the excited electron in the QD (Figure 1.12).[26]

In case this interaction between QDs and Fe(III)PPIX occurs, QDs fluorescence quenching should be seen and it could be used in order to study this interaction.

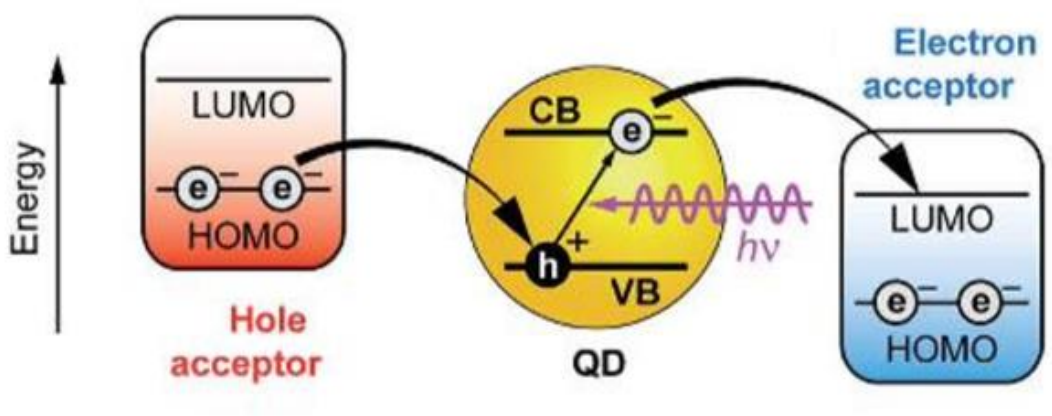

Figure 1.12. Potential charge transfer mechanism of QDs.[26] In the right part of the image is shown the possible mechanism of QD fluorescence quenching through a charge transfer reaction of an electron between the conduction band of QD and the LUMO orbital of the electron acceptor (Fe(III)PPIX working as the quencher), after the excitation of the QD electron from the valence (VB) to the conduction band (CB) by the absorption of radiation.

Thanks to this, it could be possible to study the interaction of an antimalarial drug with Fe(III)PPIX by measuring the quenching of fluorescence of QDs functionalized with this particular drug (section 1.1.4). In fact, in case of an interaction between the drug and Fe(III)PPIX, labelled QDs and haem (known to be a QD quencher) will come into contact and it would be possible to observe the quenching of QD fluorescence, proving the occurred interaction between the drug and Fe(III)PPIX.

1.3.4. Alternative analytical techniques

In addition to fluorescence emission spectra of QDs, other available techniques will be used in order to gain insights into the chemical interactions under study. UV-Vis spectroscopy, scanning electron microscopy (SEM) and transmission electron microscopy (TEM) will be used; however, the background behind each technique is beyond the scope of this project and will not be discussed in detail.

1.4. Scope

An understanding of the methods within the Plasmodium parasite's life cycle relevant to antimalarial research, namely the process of haemoglobin degradation and haemozoin formation, can be combined with the principles of fluorescence spectroscopy as applied to QD-COOHs to help solve pertinent issues in the malaria problem. In particular, this project focuses on the study of chloroquine antimalarial mechanism of action, regarding the inhibition of haemozoin formation. The relationship between Fe(III)PPIX, β-haematin and chloroquine will be investigated using QD-COOHs as the primary tool throughout this exploration.

CHAPTER 2

Aim and Objectives

2.1. Aim

The aim of this work was to study chloroquine antimalarial mechanism of action in inhibiting haemozoin formation by exploiting fluorescence emission properties of chloroquine derivative-labelled QDs to probe interactions between the antimalarial drug and Fe(III)PPIX and related compounds.

This aim was achieved through completing the following objectives:

2.2. Objectives

2.2.1 Synthesis of chloroquine derivative GG5 and characterization.

2.2.2 Gaining a comprehensive understanding of the properties and behaviour of QD-COOHs in solution using fluorescence characterization and TEM.

2.2.3 Synthesis of chloroquine-labelled QDs (QD-CQs) and characterization of products using SEM and TEM.

2.2.4 Evaluation of interactions between QD-COOHs and QD-CQs with CQ and Fe(III)PPIX using fluorescence emission spectra.

2.2.5 Synthesis of β-haematin and evaluation of its interaction with QD-COOHs and QD-CQs using TEM.

CHAPTER 3

Results and Discussion

3.1. Synthesis of Chloroquine Derivative

In order to achieve the labelling of QDs with a compound able to interact with the haemozoin crystal surface, a derivative of chloroquine (Figure 3.1), a well-known antimalarial capable of inhibiting haemozoin formation, was prepared by introducing at the tertiary nitrogen, an aminoethyl functionality: in this way, a primary amine was obtained, that could be subsequently coupled with the QDs.

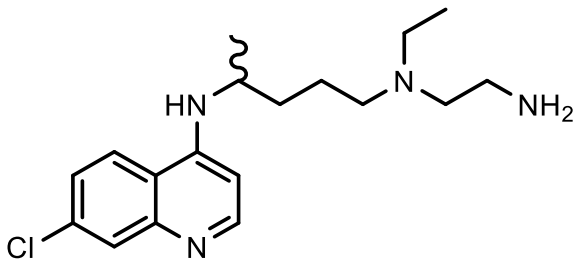

GG5

Figure 3.1. Target chloroquine derivative **GG5**.

A wide interest has been devoted in the literature to the dealkylated derivative of chloroquine (known as desethylchloroquine) as it is the major human metabolite of the antimalarial chloroquine[27], and previous studies have reported on the synthesis of this derivative.[10, 28] Therefore, the synthetic route outlined in Scheme 3.1 was followed, as disclosed in Chapter 5, with slight modifications. The chemical nature of intermediates (GG1-GG4) and final product (GG5) was confirmed by NMR analysis.

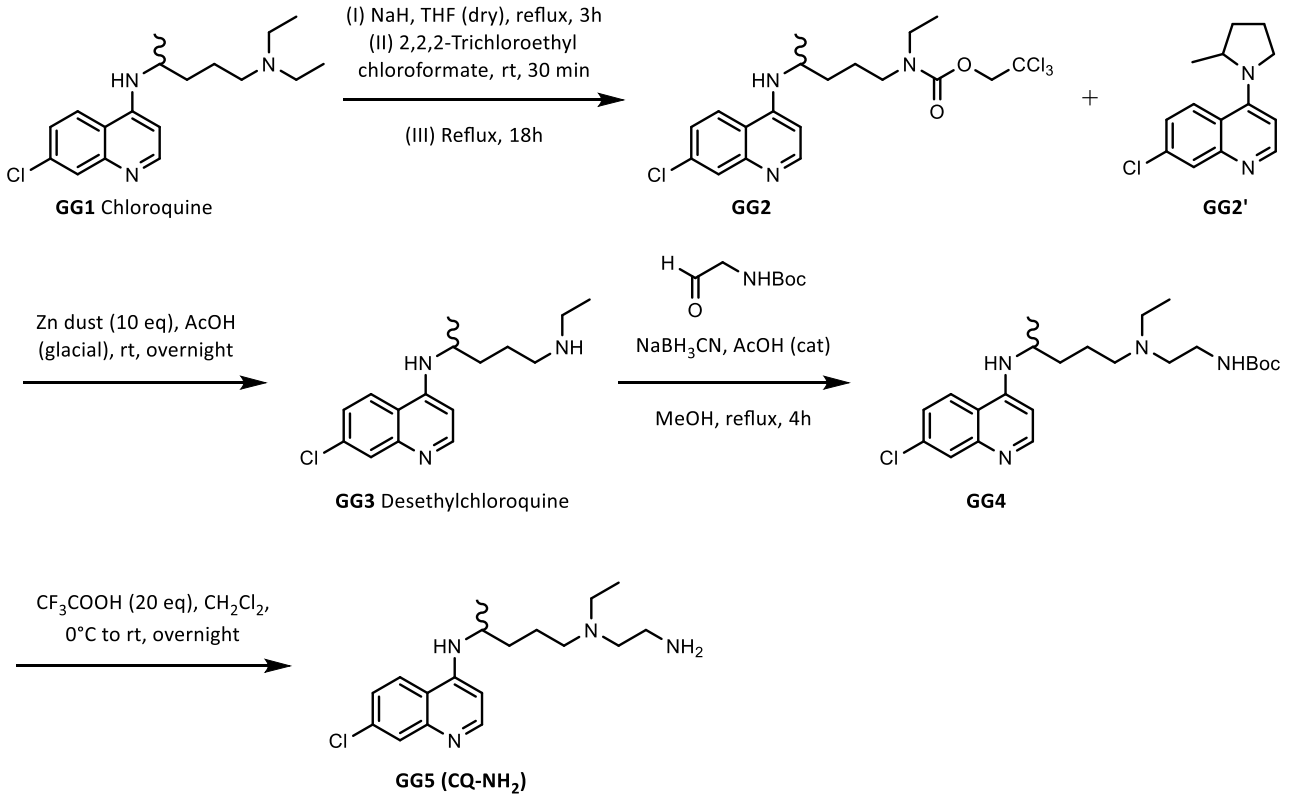

Scheme 3.1. Synthesis of chloroquine derivative **GG5**.

As can be seen in scheme 3.1, the synthesis of the chloroquine derivative involves four steps. First, the commercial phosphate salt of chloroquine was treated in order to obtain the free base, then the desethylation of chloroquine was performed by using a chloroformate, which was generated using sodium hydride and 2,2,2-trichloroethyl chloroformate in refluxing THF. Work-up and subsequent purification yielded two quinoline derivatives, GG2 and GG2', that could not be separated by column chromatography.

^{1}H NMR analysis confirmed the presence of the desired product GG2 with GG2' as co-product and, as reported in the previous work[10], the ratio between the two intermediates is approximately 2:1, according to the integration of ^{1}H NMR peaks.

The formation of the two products GG2 and GG2' could be rationalised as follows. Treatment of chloroquine with sodium hydride leads to deprotonation of the relatively acidic aromatic secondary 4-amino group (Scheme 3.2), while the tertiary amine of the side chain is N-acylated by the chloroformate, to afford a charged carbamate intermediate (depicted in square brackets). The amino anion can follow two pathways, a β-elimination on a relatively unhindered ethyl group (red

arrows), or alternatively it can act as a nucleophile at the α-methylene in the chain (blue arrows). While the former process affords the desired desethyl product GG2 as its protected trichloroethyl carbamate, the latter route affords pyrrolidine GG2' in a 5-exo-tet cyclisation.

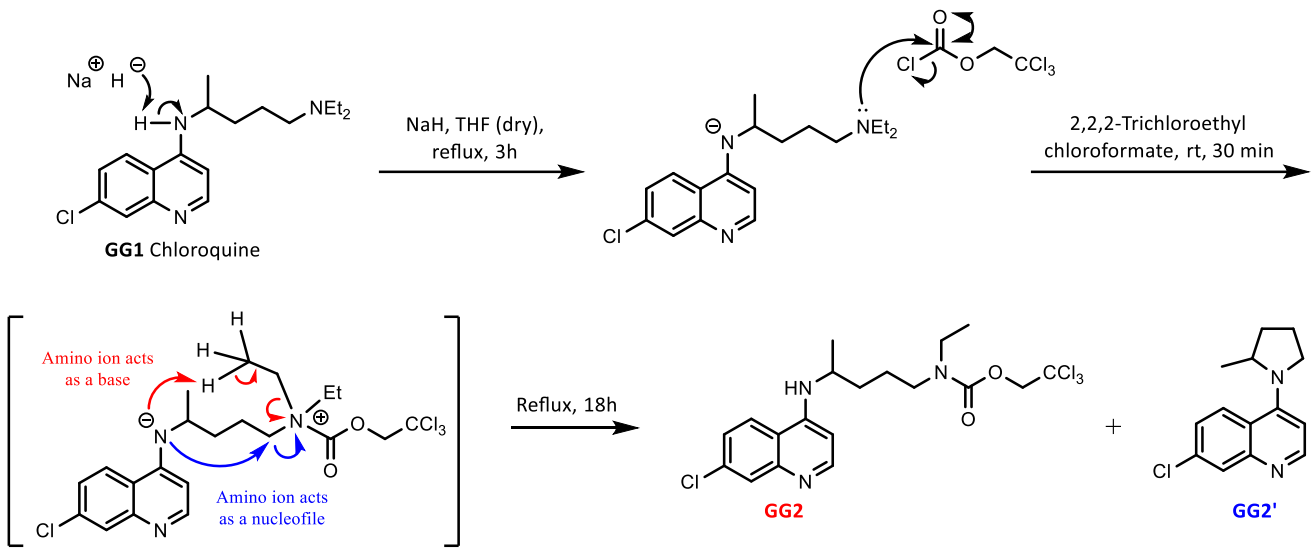

Scheme 3.2. Mechanism of formation of **GG2** and **GG2'** respectively described with red and blue arrows.

Next, the mixture of GG2 and GG2' was treated with zinc dust in acetic acid at room temperature. The purification, achieved using column chromatography, gave the target compound desethylchloroquine (GG3) in 20% yield (over two steps).

The nature of the product was confirmed by recording the ^{1}H NMR spectrum in which was observed, compared to the parent chloroquine, integration of peaks in the aliphatic area corresponding to only one ethyl group. Moreover, it is possible to observe the appearance of a broad singlet around 3.70 ppm, related to the -NH- group of the newly formed secondary amine (Figures 3.2 and 3.3).

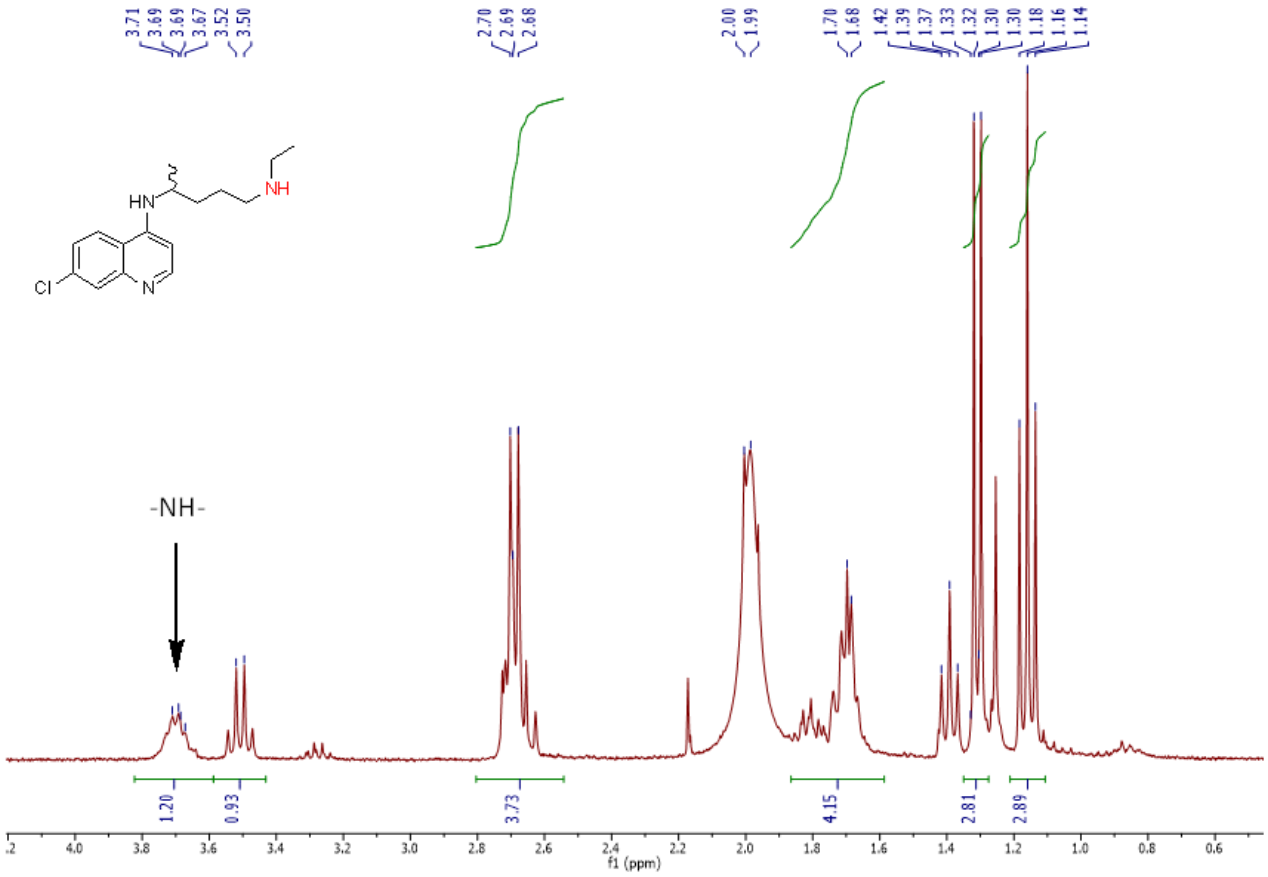

Figure 3.2. Aliphatic part of **GG3** ^{1}H NMR spectrum with novel -NH- signal outlined.

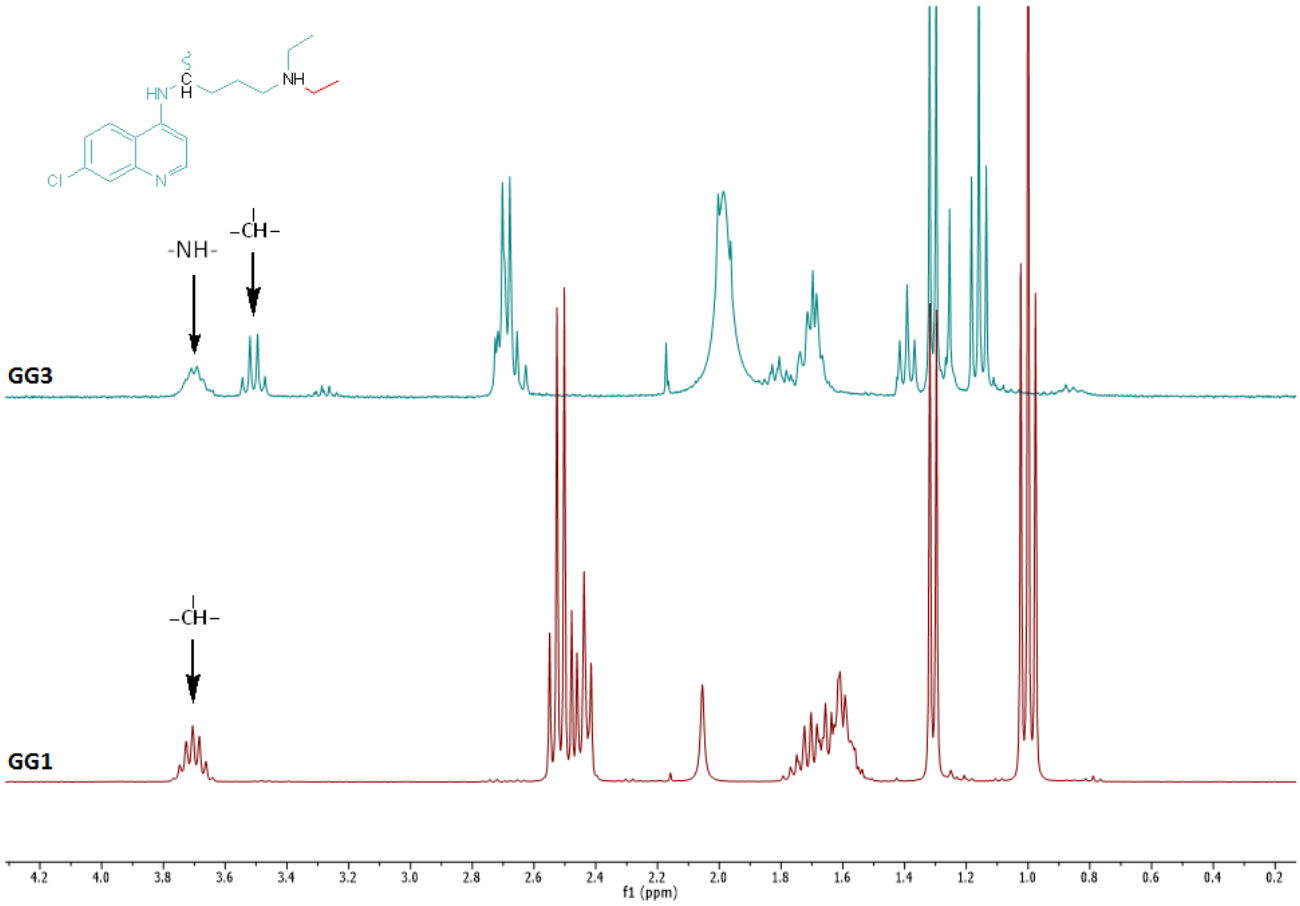

Figure 3.3. Comparison of the aliphatic areas of ^{1}H NMR spectra of **GG1** and **GG3**.

Desethylchloroquine GG3, was then N-alkylated through reductive amination with commercial N-Boc-glycinal in presence of a catalytic amount of acetic acid, in order to introduce a protected additional amine group. After refluxing for four hours, the reaction was quenched and the product GG4 extracted and purified with column chromatography (yield = 53 %).

In the ^{1}H NMR spectrum a new singlet integrating for 9H around 1.4 ppm revealed the introduction of the t-butyl group (Figure 3.4).

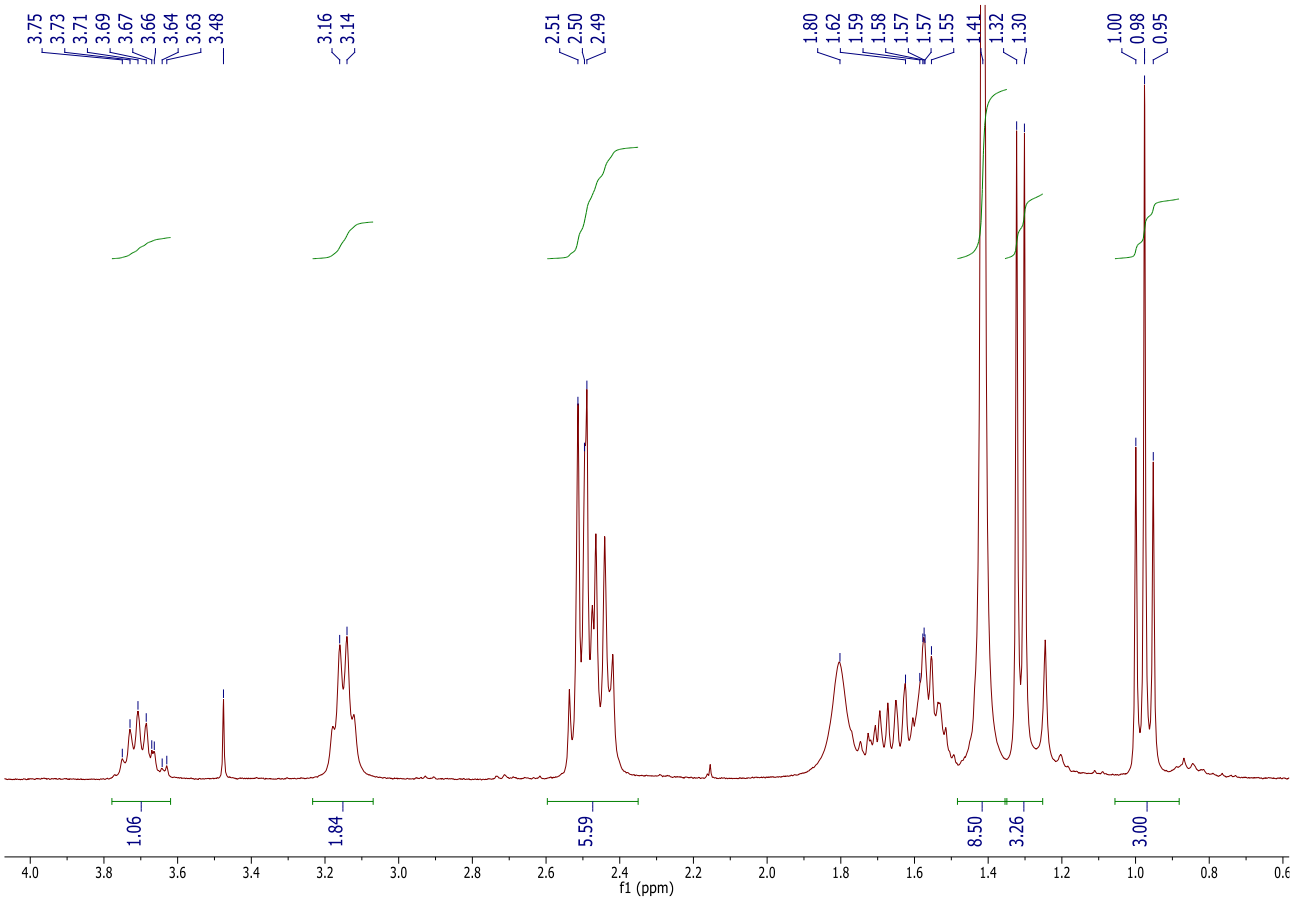

Figure 3.4. Aliphatic area of ^{1}H NMR spectrum of **GG4** in which the 9H singlet around 1.4 ppm is shown.

The reductive amination mechanism involves the formation of an iminium ion intermediate (Scheme 3.3). The secondary aliphatic amine reacts with an aldehyde under acid-catalysed conditions forming the hydroxylamine intermediate which, after a proton transfer process and the elimination of a water molecule, is converted into the iminium salt. Reduction with sodium cyanoborohydride ($NaBH_3CN$), leads to the formation of the desired product. $NaBH_3CN$, was preferred to sodium borohydride as a mild reducing agent thanks to its lower reactivity and higher stability in methanol due to the presence of the electron-withdrawing cyanide group.

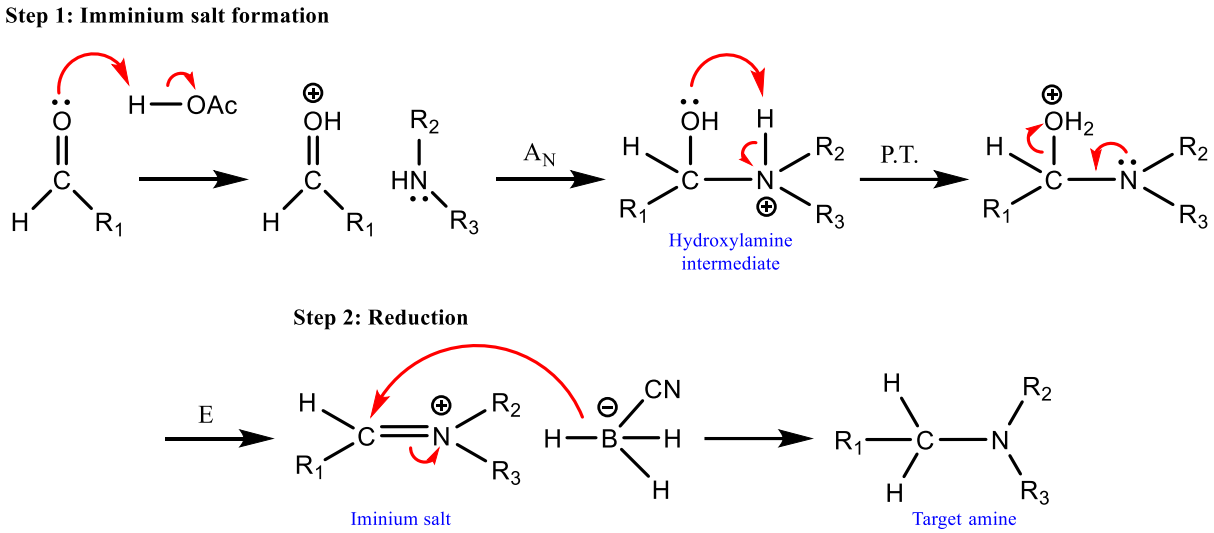

Scheme 3.3. Mechanism of formation of iminium salt and subsequent reduction with $NaBH_3CN$.

In the last step, in order to deprotect the amine and obtain the final compound, the Boc group was cleaved using an excess of TFA in CH_2Cl_2 under reflux for 8 hours. After TLC indicated the reaction was complete, the trifluoroacetate salt was treated with 1 M NaOH and extracted in dichloromethane. The product GG5 (CQ-NH_2) was then considered pure enough by HPLC (85%) to be used without any purification process also to avoid any possible degradation and stored in the dark at 4°C.

The ^1H NMR spectrum (Figure 3.5) showed the disappearance of the t-butyl signals, confirming the successful removal of the -Boc group and, together with ^{13}C NMR, the nature of the final product.

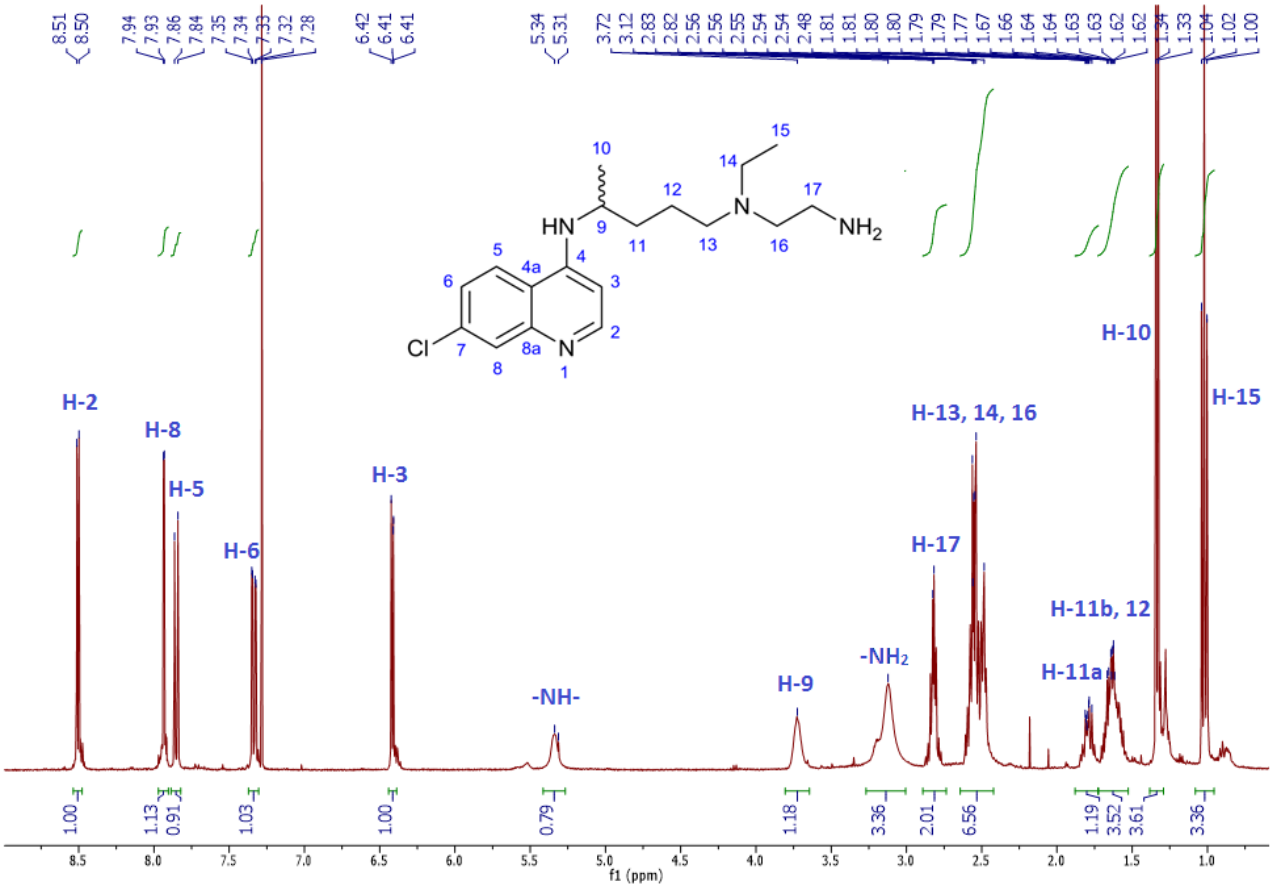

Figure 3.5. ^{1}H NMR spectrum of **GG5**.

3.2. Quantum Dots

QDs obtained from Cytodiagnostics consisted of a CdSe core covered by a ZnS shell and are functionalized with carboxylic acid ligands on the surface. The presence of these groups is fundamental for the functionalization with the primary amino group of the previously synthesized chloroquine derivative (GG5, CQ-NH_2) through the formation of an amidic bond using EDC as a coupling agent. Labelling the drug with quantum dots could be an important tool to study its interaction with the haemozoin crystal surface, exploiting the fluorescent properties of QDs.

3.2.1. Fluorescence characterization of QD-COOHs

In this work the nanoparticles with a specific emission wavelength at 630 nm, 6 nm diameter and a broad absorption spectrum used, had already employed in previous studies.[29] Optimal experimental conditions and instrumental parameters, such as excitation and emission wavelengths, photomultiplier tube voltage (PMT), scan speed and emission and excitation slit widths, were previously defined [29] and are reported in the experimental section.

In particular, for all excitation spectra the photomultiplier tube (PMT) voltage was set at 1000 V, to increase the intensity as much as possible, and the slit widths were 10 nm for excitation and 5 nm for emission to maximize the light intensity. Excitation wavelength was set at 400 nm. A 30 µL fluorescence cuvette was used in order to minimize the volume of QD-COOHs needed for each experiment.

In order to ensure applicability of the system to future biological contexts, 0.01 M HEPES (pH 7.5) buffer was chosen for following experiments despite other buffers (PBS, TRIS), exhibiting a better behaviour with 630 nm QD-COOHs in terms of maximization of fluorescence emission intensity and permitting a good solubility of Fe(III)PPIX.

For solutions containing both QD-COOHs and Fe(III)PPIX, fluorescence emission spectra may be affected by electronic interactions between the two substances. Fe(III)PPIX is a difficult compound to work with, largely due to its hydrophobicity and complicated speciation profile. Unwanted interference such as overlap between the Fe(III)PPIX UV Visible (UV-Vis) absorption spectrum and the QD-COOH fluorescence emission spectrum could result in reduction of the QD-COOH fluorescence intensity through the primary inner filter effect (pIFE). In order to evaluate this aspect,

the fluorescence emission spectrum of QD-COOHs was compared to the UV-Vis absorption spectrum of OH/H_2O-Fe(II)PPIX (haematin) in d-H_2O (Figure 3.6).

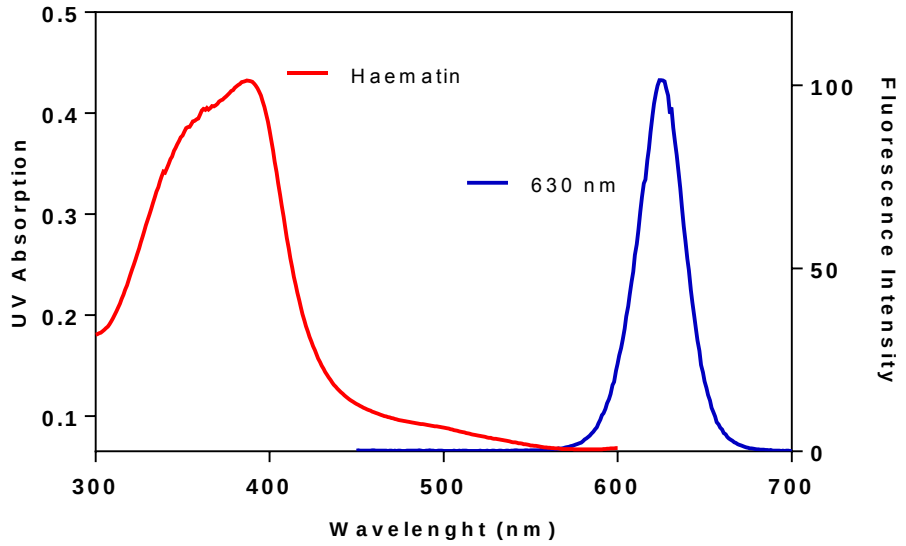

Figure 3.6. Fluorescence intensity of 630 nm QD-COOHs emission spectrum overlaid on the haematin UV-Vis absorption spectrum in d-H_2O.

The haematin absorption peak presents a maximum around 380 nm which then decreases rapidly to very low absorbance at 550 nm. The Soret band has a wide shoulder due to the formation of the π-π dimer under aqueous conditions.[30] The emission spectrum of 630 nm QDs is sufficiently far from the maximum absorption of haematin and that should ensure non-significant problems related to the primary inner filter effect.

The excitation spectrum of the QD-COOHs was also evaluated and compared with the UV-Vis absorption of haematin in order to estimate the optimal wavelength to use for this study (Figure 3.7). An excitation wavelength of 420 nm was chosen for solutions with both haematin and QDs in order to maximize the absorption of the radiation by QDs. Lower wavelengths than 300 nm were rejected to avoid the presence of a high intensity second order peak at double of the wavelength of the incident radiation as this would interfere with QDs emission spectra. Wavelengths between 300 and 400 nm were not suitable owing to the very intense absorption by Fe(III)PPIX in this range.

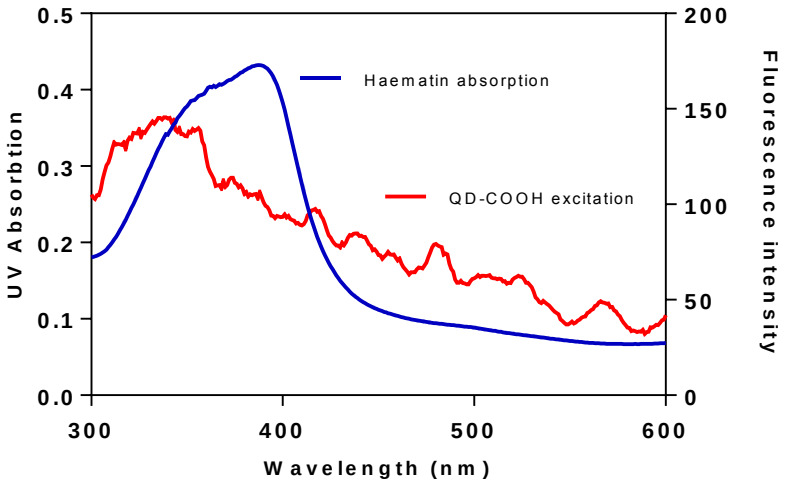

Figure 3.7. Excitation spectrum for 630 nm QD-COOH overlaid with haematin UV-Vis absorption in d-H_2O. PMT = 1000 V, Em λ_{max} = 630 nm.

3.2.2. Detection limit of QD-COOHs in d-H_2O

Due to the high cost of QDs, the minimum amount of material that could be used in further experiments was determined by evaluating the detection limit through a series of dilutions. The PMT voltage was set at 800 V.

As shown in Figure 3.8 the emission peak intensity at 630 nm decreased in a linear manner (r^2 = 0.9943) as a function of dilution from 1:10 to 1:80 and became undetectable at 1:160 dilution. In order to have a sufficient intensity, 1:20 dilution was used in further experiments.

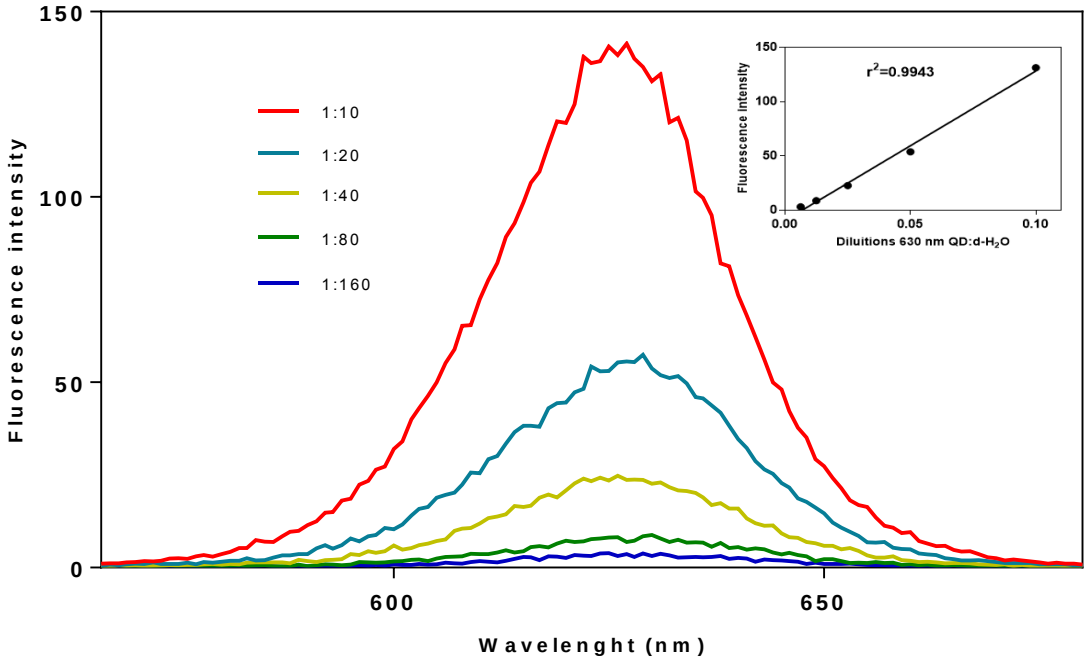

Figure 3.8. Fluorescence intensity of 630 nm QDs at various levels of dilution in water (1:10; 1:20; 1:40; 1:80 and 1:160 respectively), Insert: linear relationship between dilution and fluorescence intensity (R^2=0.9943); PMT = 800 V, Ex λ_{max} = 400 nm.

3.2.3. Transmission electron microscopy (TEM) characterization of QD-COOHs

QDs were visualised using transmission electron microscopy (TEM) (Figure 3.9). A sample of 630 nm QD-COOHs was visualised directly from the 1 mg/mL H_2O suspension obtained from Cytodiagnostics. The sample was sonicated for two minutes before being placed on a grid for analysis in order to create a homogenous suspension. The diameters of individual QD-COOHs were confirmed to be around 5-6 nm as stated by Cytodiagnostics.[24] The TEM experiments confirmed the nanoparticles tendency to aggregate, an effect which could be reversed by sonication, re-dispersing the QD-COOHs homogenously in the solution.

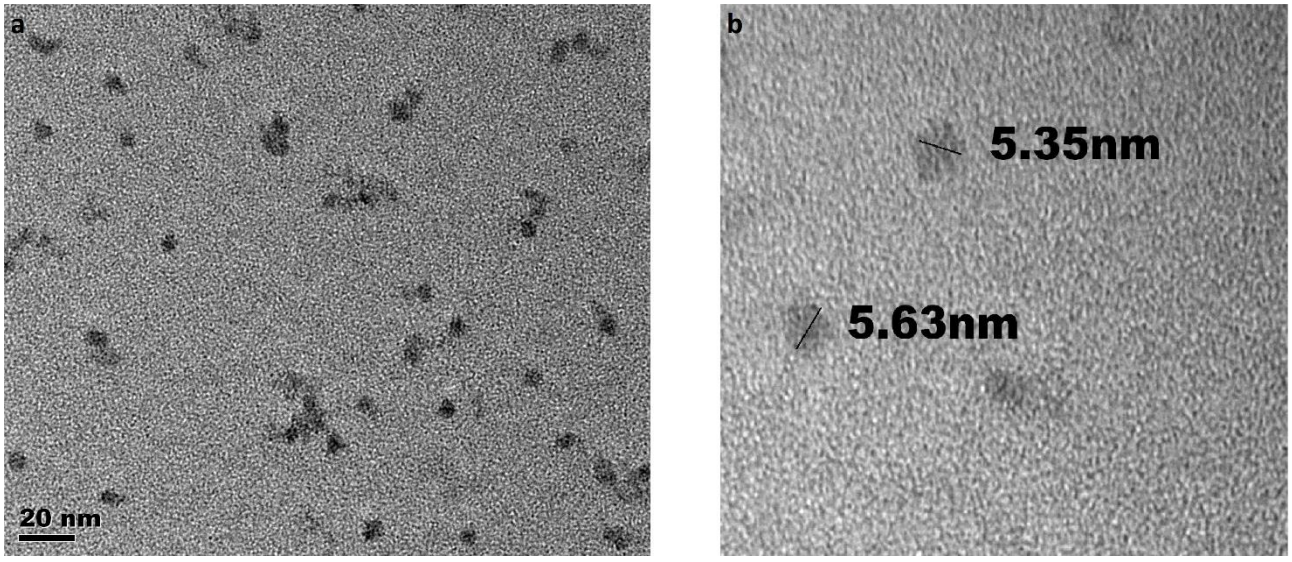

Figure 3.9. TEM images of a sample of 630 nm QD-COOHs (**a** and **b**) with two dots labelled with sizes 5.35 nm and 5.63 nm (**b**).

3.3. Derivatisation of QD-COOHs Through EDC-mediated Coupling

The principal aim of this work was to study the interactions between the chloroquine derivative GG5 (CQ-NH_2) and Fe(III)PPIX or β-haematin. In order to study this interaction, the drug was labelled with QD-COOH to take advantage of QDs fluorescence properties.

3.3.1. Synthesis of labelled QD-CQs

1-Ethyl-3-(3-dimethylaminopropyl)carbodiimide (EDC)-mediated coupling has been widely reported as a simple one-pot method to functionalize QD-COOHs.[31, 32] The coupling occurs through formation of an amide bond between the carboxylic functions on the surface of QDs and a primary amine group on the drug molecule. This molecule, a derivative of chloroquine to which is added a primary amino function through an additional alkyl chain, is expected to present similar antimalarial activity as its precursor and to behave in a similar manner with both Fe(III)PPIX and β-haematin. CQ, in fact, can tolerate multiple side chain modifications without loss of activity, and functionalization at the ethyl group termini leaves intact the 7-chloro-4-amino, quinoline pharmacophore responsible for binding to free haem and inhibiting β-haematin formation.[33]

A method adapted from *Kloepfer et al*. was used for the coupling reaction.[31, 32] The reaction brings about the formation of the amide bond in a two step procedure as shown in Scheme 3.4.

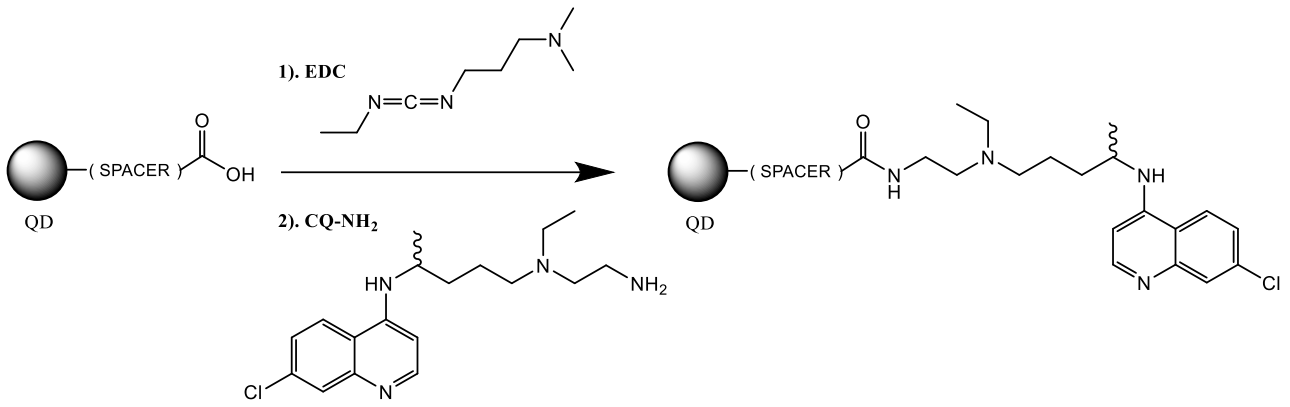

Scheme 3.4. EDC-mediated coupling between QD-COOH and CQ-NH_2.

The primary nucleophilic amine (NH_2) of the CQ-NH_2 attacks the carboxylic groups of the QDs, leading to the formation of an amide bond. In order to facilitate the reaction, the carbonyl group requires activation using a coupling mediator.

The proposed mechanism (Scheme 3.5) begins with activation of the carboxylic carbon on the QD-COOH surface with EDC (Step 1). During the activation process a proton is transferred from the carboxyl group to a nucleophilic nitrogen of EDC. The deprotonated oxygen then attacks the electrophilic carbon centre on EDC. The intermediate presents a carbonyl group activated towards nucleophilic attack. Then the primary amino nitrogen of CQ-NH_2 attacks the electrophilic carbon in a nucleophilic substitution reaction at the acyl centre (S_NAc), provoking the expulsion of a urea derivative of EDC (Step 2). The final QD-CQ product is then formed after a proton transfer process.

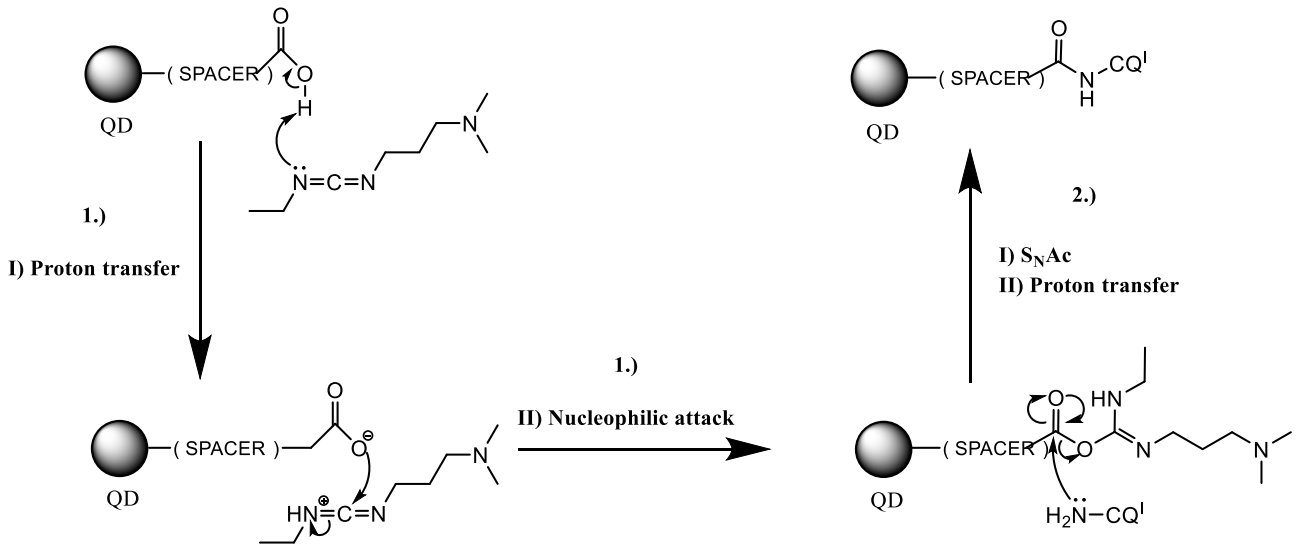

Scheme 3.5. Proposed mechanism for the EDC-mediated coupling between the QD-COOH and CQ'-NH_2.

The final product (QD-CQ) was then purified through extensive washing with 0.01 M HEPES buffer (pH 7.5). After each washing and subsequent centrifugation, the product was separated by removing the supernatant, which contains unreacted materials.

In order to monitor the presence of unreacted reagents in the supernatant, UV visible spectra were recorded after each washing. The chloroquine derivative and EDS were used in large excess during the reaction to maximize the derivatisation of the QDs, as the number of possible carboxylic acid reaction sites on each QD-COOH is unknown. As a result, a large amount of unreacted derivative was detected in the supernatant. Washing continued until the UV visible spectrum showed no reagent present in the supernatant (Figure 3.10).

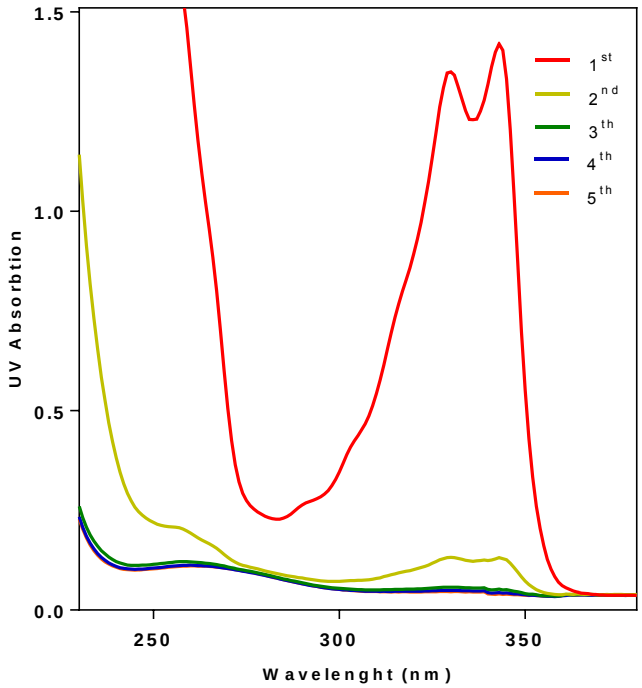

Figure 3.10. UV visible spectra of supernatant of successive (1st, 2nd, 3rd, 4th, 5th) washings.

3.3.2. Characterization of coupled QDs

Conventional methods of characterization such as nuclear magnetic resonance (NMR) and Fourier-transform infrared spectroscopy (FTIR) were not suitable to study the labelled QDs, since the QD tumbles very slowly and can be expected to cause extreme broadening of NMR peaks. Furthermore, there was far too little material for either NMR or FTIR.

In addition to fluorescence characterization, to investigate the effect of coupling on the QDs fluorescence properties, transmission electron microscopy (TEM) was also used to visualize the morphological aspect of labelled QDs. Further, scanning electron microscopy (SEM) was used to confirm the successful coupling of QDs with the drug. In particular EDS was employed to detect the presence of Cl atoms in the material. This arises only from the chloroquine derivative, which is the sole source of Cl in the sample.

The fluorescence emission spectrum of the 630 nm QD-CQ product suspended in 0.01 M HEPES (pH 7.5) was recorded. As expected, the QDs fluorescence emission peak is specifically tuned due to its size and composition so it was not affected by surface substituents.[25] On the other hand, the presence of the coupled molecule on the surface cause a decrease in the intensity of the emission peaks. Since this appeared to become worse over time it was suspected that it was probably due to an increased tendency to aggregate.

TEM was used to investigate the physical appearance of QD-CQs in a similar manner to the QD-COOHs. A sample of 630 nm QD-CQs was vortexed briefly before being placed on a carbon grid for analysis. After drying under a heat lamp, the sample was visualized using TEM (Figure 3.11).

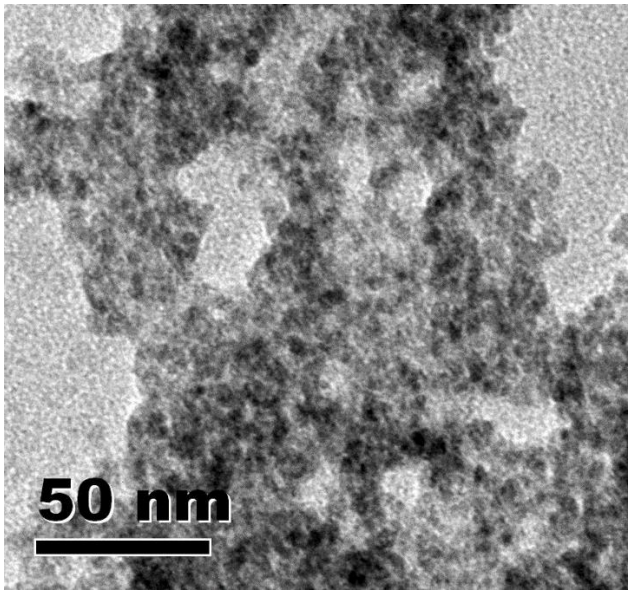

Figure 3.11. TEM image of labelled QDs showing aggregation.

As suspected from fluorescence measurements, TEM images confirmed the formation of aggregates of labelled nanoparticles, differently to what seen for unlabelled QDs.

Finally, to demonstrate that the coupling reaction had taken place, a sample of the product was analysed by SEM. It should be noted that the resolution of SEM was not adequate to detect individual QDs. Rather, this technique could detect bulk properties of a very small quantity of material. Using the EDS technique, it was possible to demonstrate the presence of the chloroquine

derivative since it was the only source of Cl in the material and it was completely absent from the underivatized QDs (Figure 3.12).

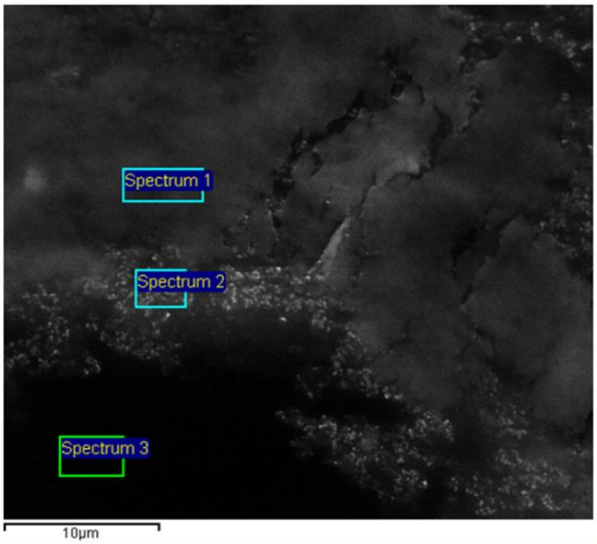

Labelled QDs

Spectrum	In stats.	S	Cl	Zn	Se	Cd	Total
Spectrum	1	26.66	1.06	47.4	8.6	16.28	100
Spectrum	2	100	0	0	0	0	100
Spectrum	3	0	0	0	0	0	0

Unlabelled QDs

Spectrum	In stats.	S	Cl	Zn	Se	Cd	Total
Spectrum	1	20.69	0	55.88	5.42	18.01	100
Spectrum	2	20.84	0	54.51	5.51	19.13	100

Figure 3.12. SEM analysis of QD-CQs and QD-COOHs with EDS report confirming the successful coupling.

Presence of QDs in the part of the SEM image at which measurements were obtained could be seen by non-zero readings for Zn and Cd. In the control, no Cl was detected, whereas in the derivatised QDs, Cl was present. SEM analysis thus demonstrated the presence of Cl atoms, belonging to chloroquine derivative GG5, on the surface of labelled QDs while it was absent on unlabelled nanoparticles (QD-COOHs).

3.4. Interactions of QD-CQs with CQ, Fe(III)PPIX and β-haematin

3.4.1. Behaviour studies of QD-CQ

Additional studies were done to investigate the effect of the functionalization on the behaviour of QDs, focusing, in particular, on the trend to aggregate.

During fluorescence experiments, QD-CQ samples were kept in the dark in the fridge at 4°C in order to prevent photobleaching. However, while performing experiments it was observed that the intensity of the fluorescence emission spectra of same samples of labelled QDs was not consistent over long time periods. This phenomenon was not noted during similar experiments on QD-COOHs, thus indicating that the stability of the QDs had been altered after coupling to the drug and the probable source of this instability was identified as aggregation of QD-CQs.

In particular, fluorescence emission intensity of both labelled and unlabelled QDs was evaluated before and after 4 hours during which the sample was kept in the dark at room temperature. The same experiment was then repeated only for QD-CQs by adding to the solution in which the nanoparticles were suspended a small amount of different solvents, such as ethanol, methanol and acetone, to see if in presence of a less polar system the tendency to aggregate could decrease, due to a possible better solvation of drug molecules present on the surface of nanoparticles and a weaker interaction between them. Unfortunately, no substantial differences were observed in the decrease of intensity of fluorescence for aggregation.

Another variation of the same experiments was done, both for labelled and unlabelled QDs, by evaluating the decrease of fluorescence emission intensity in more acidic conditions. Nanoparticle samples were diluted using a 0.01 M HEPES at pH 4.2. Under these particular conditions the intensity decreased less than in other cases as the lower pH could be disturb the process of aggregation. This was probably a result of the protonation of the CQ groups resulting in electrostatic repulsion between the QDs.

3.4.2. Spectrophotometric titrations of QD-COOHs and QD-CQs with CQ and Fe(III)PPIX

After investigating the properties and behaviour of the QD-COOH (section 3.2) and the QD-CQ (sections 3.3.2 and 3.4.1) in solution, the next step was to evaluate and compare their interactions with the compounds of interest to this project: CQ and Fe(III)PPIX.

Spectrophotometric titrations were carried out by adding to a suspension of quantum dots in 0.01 M HEPES (pH 7.5), the quencher (CQ or Fe(III)PPIX) and recording fluorescence emission spectra.

In all the four cases, a decrease of the fluorescence intensity was seen, indicating that quenching processes occurred in each system. In order to realize a preliminary investigation of the quenching processes, data were analysed using Stern-Volmer plots as explained in Chapter 1 by plotting the ratio I_0/I of the intensities observed at the maximum of QDs emission spectrum against the concentration of the quencher.

3.4.2.1. Spectrofluorometric titrations of QD-COOHs with CQ

As shown in Figure 3.13, for QD-COOHs titration with CQ, a parabolic trend is present. The parabolic trend is due to the presence of both dynamic and static quenching. The presence of static quenching in this case could be explained by the formation of an electrostatic complex between the negatively charged QD-COO^- groups and CQH_2^{2+}, positively charged by the protonation of its basic sites.

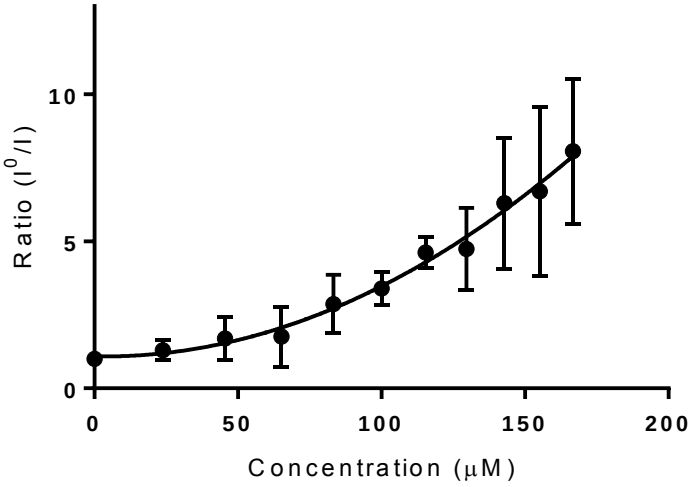

Figure 3.13. Graph showing the upward trend for QD-COOHs titrated with CQ.

3.4.2.2. Spectrofluorometric titrations of QD-COOHs with Fe(III)PPIX

Like the previous case, also for the titration of QD-COOHs with Fe(III)PPIX (Figure 3.14) a definite curvature can be observed, outlining the presence of the two quenching processes at the same time.

The static quenching, due to the formation of a non-fluorescent complex, is probably caused by the coordination of Fe(III) by QD-COO^- functionalities.

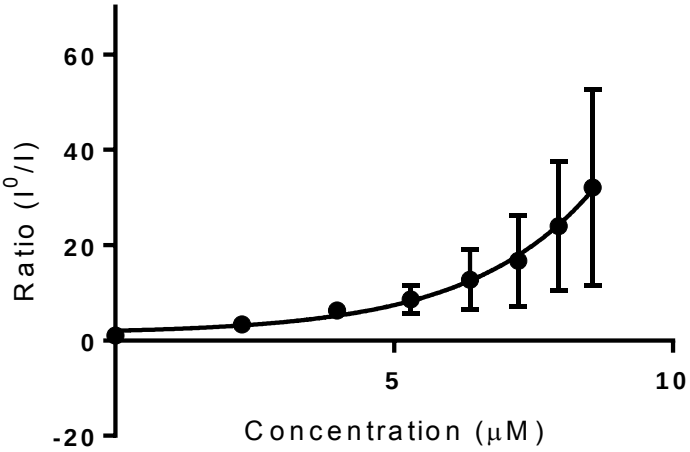

Figure 3.14. Graph showing the upward trend for QD-COOHs titrated with Fe(III)PPIX.

3.4.2.3. Spectrofluorometric titrations of QD-CQs with CQ

For nanoparticles labelled with the chloroquine derivative and titrated with CQ, as expected a linear trend is observed in the graph below (Figure 3.15). In fact, between QD-CQs and CQ, both positively charged by protonation, only pure collisional quenching can take place without any static interaction, following the Stern-Volmer plot.

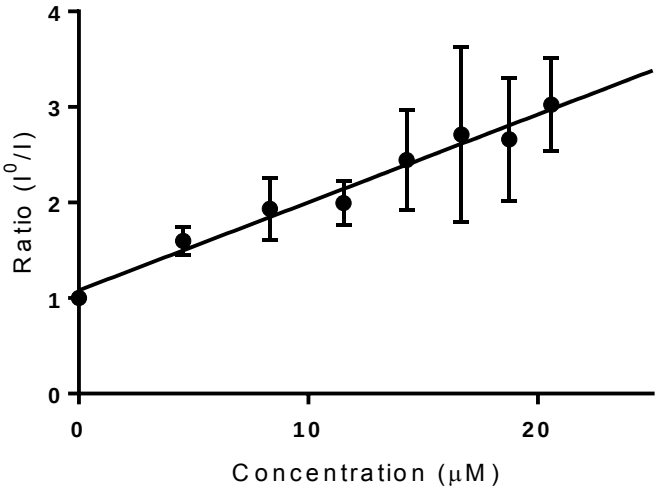

Figure 3.15. Graph showing a linear trend for QD-CQs titrated with CQ.

3.4.2.4. Spectrofluorometric titrations of QD-CQs with Fe(III)PPIX

Finally, for QD-CQs titrated with Fe(III)PPIX a linear trend was observed (Figure 3.16). In this kind of analysis, as explained in Chapter 1, a linear trend could arise from two different scenarios. The quenching could be purely dynamic, without the formation of the complex, or purely static due to an interaction of binding between QD-CQs and haem. In support of the first possibility there is the fact that in case of the formation of a complex, is strange that no dynamic quenching is observed (as in case of QD-COOHs titrated with haem). On the other hand, chloroquine and its derivative are expected to interact with haem.

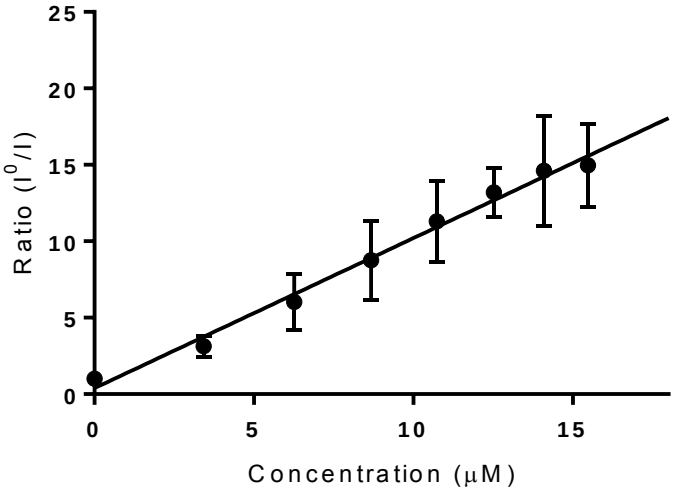

Figure 3.16. Graph showing a linear trend for QD-CQs titrated with Fe(III)PPIX.

In conclusion, these measurements permit only a preliminary analysis and is not possible to make a final conclusion. This could be reached by studying the excited state life time of QD-CQs in presence of the quencher in order to define the nature of the quenching process.

3.4.3. Synthesis of β-haematin

As mentioned in Chapter 1, even though the studies of the interaction between CQ and Fe(III)PPIX using the QD-CQs could be interesting due to the link between haem released during haemoglobin degradation and β-haematin formation[34], the target which can be used to understand the antimalarial mechanism of CQ based drugs is not believed to be Fe(III)PPIX, but β-haematin, the synthetic form of haemozoin crystals. CQ has been proven to inhibit the formation of β-haematin but the mechanism of this inhibition remains largely unknown. One possible theory explains the CQ inhibition of β-haematin crystal formation through the absorption of the drug onto the fastest growing face of the crystal. A direct study of the difference in interactions between QD-COOHs and QD-CQs with β-haematin could therefore help shed new light on this mechanism.

β-haematin was synthesized in a 9.7 M acetate buffer and the product was characterized using both PXRD and FTIR looking for the key diagnostic peaks indicated at 1660 cm^{-1} and 1210 cm^{-1}. These peaks are due to the coordination of the Fe(III)PPIX carboxylate group to the Fe^{3+} centre which splits the original signal at 1700 cm^{-1} into two asymmetric signals (Figure 3.17).

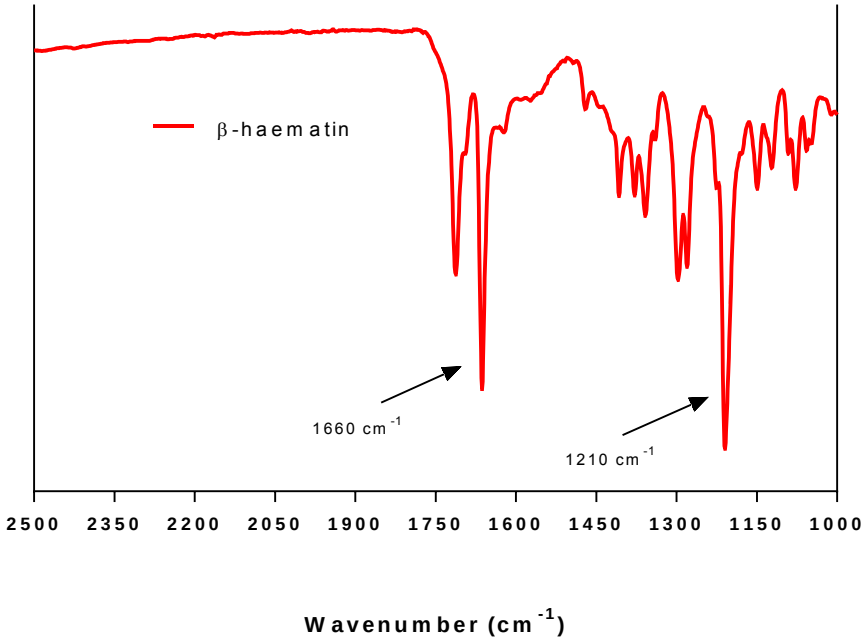

Figure 3.17. FTIR spectrum of β-haematin with peaks at 1660 cm^{-1} and 1210 cm^{-1} marked.

TEM was also used to confirm formation of β-haematin crystals by visualising a sample of the product directly under the electron microscope. The rod-like structure seen in Figure 3.18 is characteristic of β-haematin with average sizes 0.5 µm as previously reported with this method.[35]

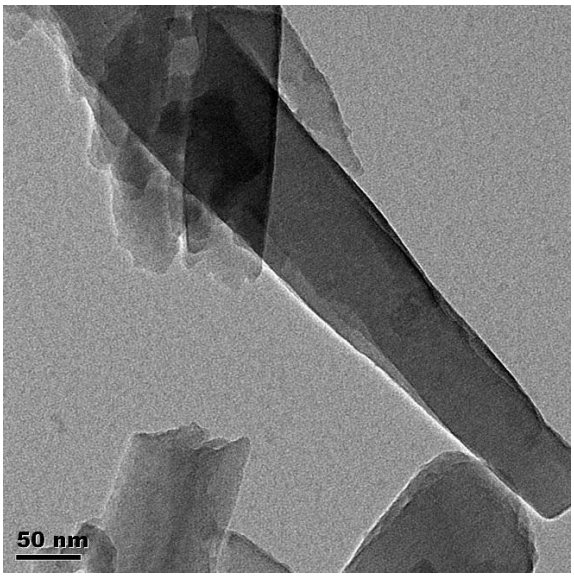

Figure 3.18. TEM image of β-haematin crystals confirming formation of product

3.4.4. Transmission electron microscopy analysis of interactions of QD-COOH and QD-CQ with β-haematin

The formation of haemozoin crystals is part of the defence mechanism used by the *Plasmodium* parasite to protect itself from toxic levels of free Fe(III)PPIX. In order to study the drug's mechanism of antimalarial activity, the interaction between the QD-CQs and β-haematin was investigated.[34] As β-haematin is a crystalline material, it was not possible to investigate its interaction with labelled QDs using fluorescence emission in solution, while TEM can be used to directly visualise the interaction between crystal surface and labelled QDs.

Control samples were prepared for visualisation by adding β-haematin to a suspension of 630 nm QD-COOHs in 0.01 M HEPES (pH 7.5). The sample was vortexed briefly in order to ensure thorough mixing but was not sonicated as the forces between the QD-COOHs and the β-haematin crystal were considered capable of being broken apart by sonication. The QD-COOHs were clearly identified in the resultant TEM image and they showed no selectivity in binding β-haematin crystals (Figure 3.19). This was expected since although the carboxylic acid ligands are negatively charged and could

coordinate to the iron centre they are unlikely to disrupt the Fe(III)PPIX dimers of β-haematin and the association is largely expected to arise from a weak electrostatic interaction.

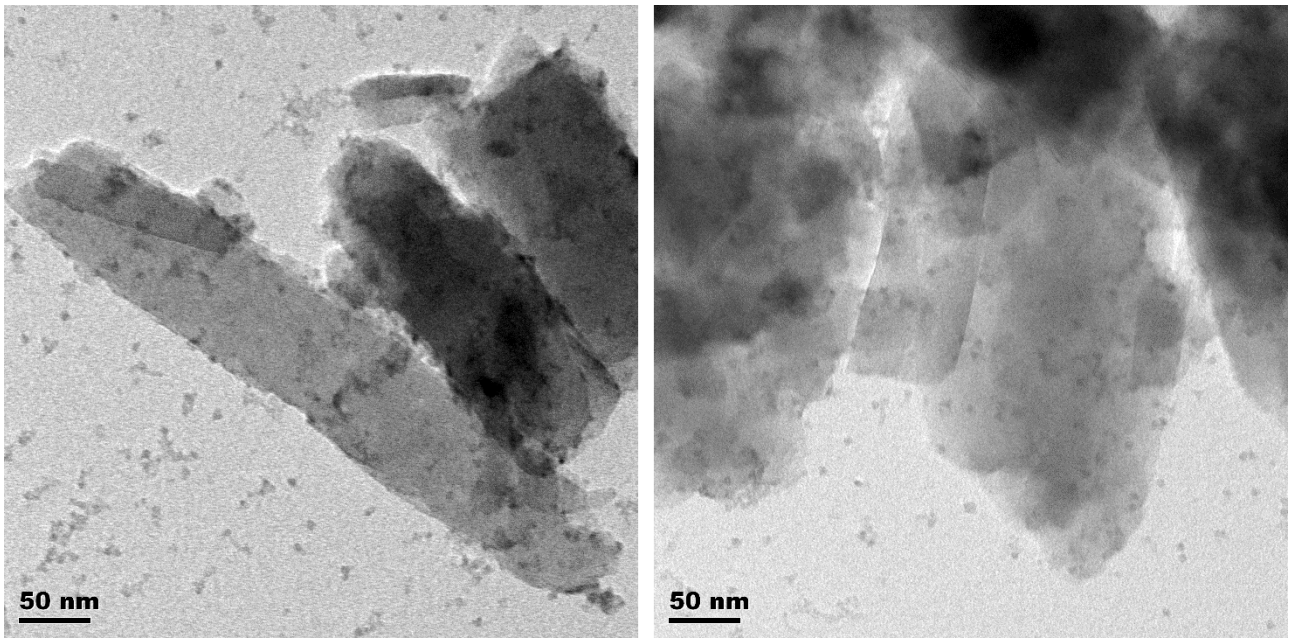

Figure 3.19. TEM images of 630 nm QD-COOHs and β-haematin crystals with no selectivity shown in binding.

The same procedure was then repeated for the QD-CQs and β-haematin. This time, QD-CQs appeared to be selective in their binding to specific faces of the β-haematin crystal with highly concentrated regions (Figure 3.20). This tendency to bind selectively specific faces was observed across many different crystals, indicating that an interaction occurs at that face.

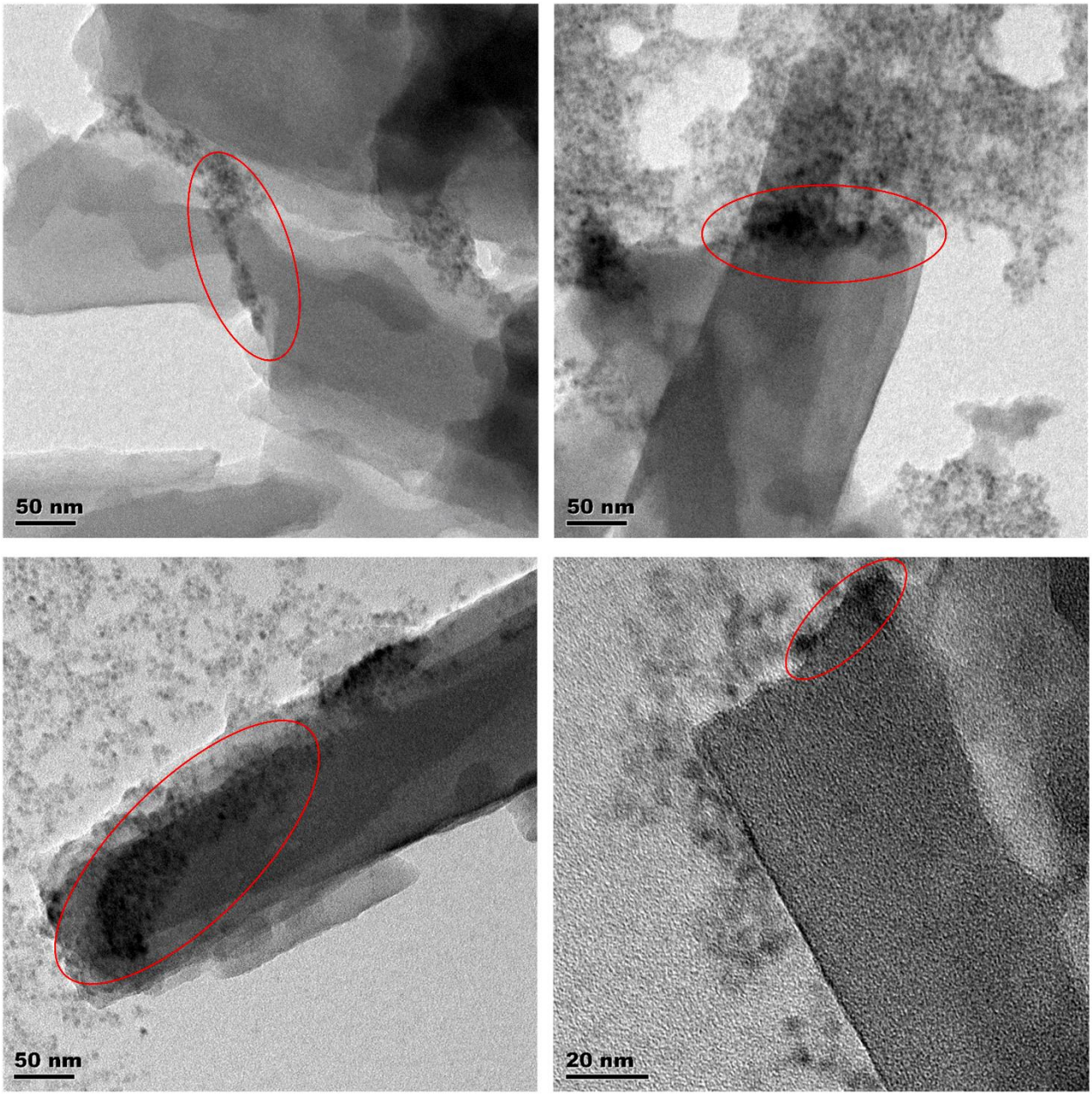

Figure 3.20. TEM images of different crystals within one sample of 630 nm QD-CQ and β-haematin, showing darker areas in which nanoparticles interact with a specific face of the crystal (red circles).

In Figure 3.21 (**a** and **b**) below, the proposed interaction between the drug and the crystal that is thought to occur on the (001) face of β-haematin crystals. This is a reproduction of a figure from a review by Weissbuch and Leiserowitz[35] and is a result of crystal structure growth and kinetics study on β-haematin. The (001) face indicated is the fastest-growing face of the crystal. A proposed

mechanism of β-haematin inhibition by CQ is through adsorption to this (001) face of the crystal as shown schematically in Figure 3.21 (**c**) adapted from Gildenhuys 2013.[16] The TEM images collected in this work (Figure 3.20) supply further evidence of CQ adsorption to the fastest-growing face of the β-haematin crystal as described by the above mentioned theory.

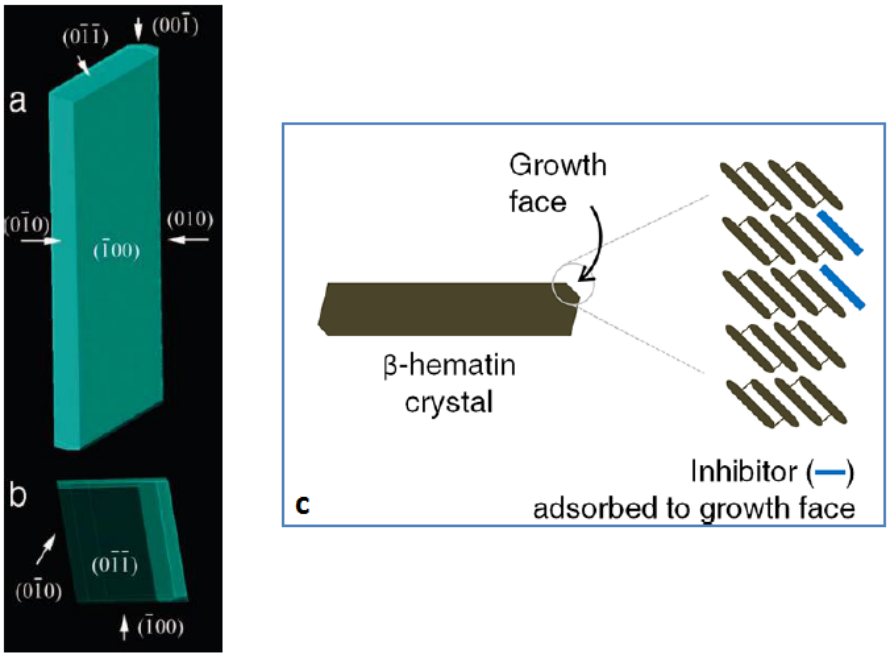

Figure 3.21. (a) and **(b)** Theoretical growth form of β-haematin as viewed along the *a*- and *c*- axis respectively by Weissbuch and Leiserowitz[35] and **(c)** Schematic illustration of the formation of a drug monolayer on the surface of a β-haematin crystal by adsorption to binding sites on the growth face adapted from Gildenhuys.[16]

CHAPTER 4

Conclusions and Future Work

4.1. Conclusions

The aim of this project was to investigate the mechanism of action of the antimalarial drug chloroquine by using QD-COOHs in order to exploit their particular fluorescence properties. This was accomplished by coupling a CQ derivative and the QD-COOH, obtaining a stable CQ-labelled fluorophore (QD-CQ). Despite the fact that CQ is known to act as an inhibitor of haemozoin formation, its detailed mechanism of action is still largely unproven, so this was an attempt to contribute towards its elucidation. In order to investigate CQ action, regarding the two main hypothesis presented in Chapter 1, interactions of the drug have been evaluated with β-haematin, the synthetic equivalent of haemozoin, and Fe(III)PPIX, as a product of the haem degradation process and starting material for the formation of haemozoin crystals within the Plasmodium parasite's DV in a human host's RBCs.

The synthesis of chloroquine derivative (GG5) has been achieved successfully by following the procedure reported in the experimental section.

QD-COOHs have never been used to investigate interactions between Fe(III)PPIX and CQ, therefore part of this work has been involved in studying their applicability to this system. Helpful considerations have been derived by a similar study[29], previously carried out in the same research group, concerning the use of QDs in studying quinidine's mechanism, a different antimalarial drug. QD-COOHs fluorescence emission properties have been confirmed and 0.01 M HEPES (pH 7.5) buffer was chosen to be used in the rest of the project thanks to its good ability to disperse both the QD-COOH and dissolve Fe(III)PPIX without unnecessary fluorescence quenching. The UV-Vis absorption of haematin was also confirmed to have minimal interference with the fluorescence emission peaks of the QD-COOHs which decreased the incidence of the primary inner filter effect (pIFE) due to absorption of light by Fe(III)PPIX.

The interaction between the QD-COOH and both CQ and Fe(III)PPIX was characterized through fluorescence quenching of the QD-COOH emission peak as a result of spectrofluorometric titration with CQ and Fe(III)PPIX. As observed in the previous study the nature of this interaction is quite complex. The selectivity of the QD-COOH associations was difficult to confirm and further investigations are necessary in order to gain a better understanding of the system.

The coupling between the QD-COOH and CQ derivative was achieved through a simple and easily reproducible method. This EDC-mediated coupling permitted the formation of an amidic bond between the primary amino chain of the drug and carboxylic groups on QDs surface. Characterization of the QD-CQ product was mainly carried out by using SEM with EDS technique in order to detect the presence of CQ's Cl on QDs surface. In addition, evaluation of its fluorescence emission spectra and comparison between its interactions with CQ and Fe(III)PPIX and those of the unlabelled QD-COOH proved to be a useful method of characterization. TEM was also used to visualise the physical appearance of both the QD-COOH and QD-CQ.

Although QD-CQs were easily synthesized, their stability and behaviour in solution was not as good as those of the QD-COOHs. Problems were encountered with aggregation of QD-CQs which caused unwanted fluorescence emission quenching and lack of reproducibility of results. Aggregation was able to be partially reversed through sonication of samples for two minutes. Fluorescence emission peaks of QD-CQs also decreased over time when the samples were kept at room temperature (20˚C), but this was partially solved by storing the samples in the dark at 4˚C between measurements.

Evaluation of the fluorescence emission spectra of the interaction between the QD-CQs and Fe(III)PPIX in solution was not completely clear and the data analysis using Stern-Volmer plot keeps open two possible scenarios about the nature of the quenching process, dynamic or static quenching. Further investigation measuring the fluorescence life times (τ) could be useful to clarify the mechanism of the process.

β-Haematin was successfully synthesised in 9.7 M acetate solution and crystals characterized through PXRD and FT-IR. The interaction between these crystals and both labelled and unlabelled QDs was studied by using TEM. The comparison between them showed specific binding of the QD-CQs in particular to the end face of the β-haematin crystal, probably the (001) face, which was not seen with the unlabelled QD-COOHs which were randomly dispersed over crystal surface. Adsorption of CQ onto the fastest growing face of the crystal, specifically the (001) face, has been suggested as its mechanism of action, but this theory has not yet been conclusively proven. The TEM

images of the QD-CQs interacting with this face of β-haematin thus provide new evidence supporting this theory.

Although some complications arose in using QD-COOHs to probe the binding interactions of CQ with Fe(III)PPIX, this study has shown that they are a potentially powerful tool in giving new insights into the mechanism of β-haematin inhibiting antimalarials.

4.2. Proposed Future Work

A challenge in this project was controlling the fluorescence emission and stability of the QD-COOHs. They were obtained from Cytodiagnostics and their core size, composition (CdSe with a ZnS core-shell with a capping carboxylic acid ligand) and their set emission wavelength are all known.[24] The specific nature and quantity of the carboxylic acids was unknown, which presented difficulties in interpretation of results when investigating their binding. A proposed solution to this would be to synthesise QDs of known composition *de novo*. This would allow for further fine-tuning of chemical properties as well as afford a larger amount of material at a smaller cost, which was another limiting factor.

Synthesising QDs would also allow modifications to be made for better applicability in studying Fe(III)PPIX and related compounds as part of antimalarial research. Although the carboxylic acid functionalised ligands render the QDs easily capable of forming new covalent bonds, as was demonstrated by coupling to a CQ derivative, in a preceding study their permeability into RBCs was found to be poor and this could limit their applicability in studying living systems. This difficulty with QD-COOHs has been previously reported and CdSe/ZnS QDs with PEG-ylated ligands are proposed as a solution.[36, 37] Leaching of Cd^{2+} ions can also occur from the QD core which makes these QDs potentially highly toxic.[36] Although this effect was not encountered here as the QD-COOHs were not used in living cells (and were suspended in aqueous media at all times to limit exposure), further investigation could be done into the possible synthesis of environmentally friendly alternatives.

In terms of the results of applying QDs and their physical and electronic properties to investigating the antimalarial mechanism of CQ, this work has shown the promising application as investigation tools, despite some problems which could be solved in the future.

In particular, the great tendency to aggregate of labelled QDs represent a remarkable obstacle to their application. Further studies would be necessary to improve their stability and the reproducibility of related measurements. A possible solution could be the partial functionalization of surface carboxylic groups with molecules which could help to improve solubility or, to repulse each other, to avoid aggregation.

The analysis of titration data to study the interaction between QD-CQs and Fe(III)PPIX did not lead to a definitive conclusion. As already mentioned, the study of fluorescence life times (τ) of QDs in presence and absence of the quencher (Fe(III)PPIX) would be necessary to clarify if the observed quenching processes belong to the dynamic or static type.

The TEM experiments done with the QD-CQ also showed promising evidence of CQ adsorption onto the fastest growing crystal face of β-haematin. The methods used to lead up to both of these results need refinement, but with a better understanding and control of the QD's properties they could become reliable and powerful tools in helping to better understand the mechanism of action of haemozoin inhibiting antimalarials.

CHAPTER 5

Experimental

5.1. Synthesis of Chloroquine Derivative

5.1.1. General methods and instrumentation

Unless otherwise stated, all reagents were purchased from Sigma-Aldrich and used without further purification. Solvents were purchased from Kimix Chemicals. Anhydrous $CHCl_3$ and CH_2Cl_2 were freshly distilled over $CaCl_2$ and P_4O_{10}, respectively. THF was distilled from sodium wire and benzophenone. Double-distilled deionised water (dH_2O) was provided by a Millipore Direct-Q3 water purification system.

Thin-layer chromatography (TLC) was carried out on aluminium-backed silica gel 60 F254 plates (Merck). Compounds were visualised under short-wavelength UV light (254 nm) or long-wavelength UV light for fluorescence detection (365 nm). For staining, plates were sprayed with a 2.5% solution of anisaldehyde in a mixture of sulphuric acid and ethanol (1:10 v/v) or with a 0.3% solution of ninhydrin in absolute ethanol acidified with 3% glacial acetic acid.

For column chromatography, silica gel with pore size 60 Å and particle size 35-70 µm was used. Occasionally, flash chromatography was performed using a Biotage Isolera (silica gel with pore size 60 Å and particle size 63-200 µm).

Nuclear magnetic resonance (NMR) spectra were recorded on Bruker 300 or 400 MHz spectrometers. Chemical shifts were recorded relative to residual chloroform in $CDCl_3$ (δ 7.26 ppm in ^1H NMR and δ 77.16 ppm in ^{13}C NMR).

High performance liquid chromatography (HPLC) was performed using an Agilent 1220 LC System VL equipped with an Agilent ZORBAX Eclipse Plus C18 column (5 µm, 4.6 mm x 150 mm). Compounds dissolved in acetonitrile (0.3 mg/mL) were run at a flow rate of 1 mL/min with UV detection at 254 nm.

5.1.2. N^4-(7-chloroquinolin-4-yl)-N^1,N^1-diethylpentane-1,4-diamine, chloroquine free base (GG1)

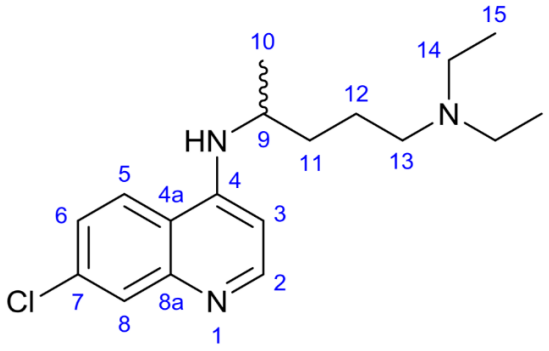

Chloroquine diphosphate was converted to the corresponding free base by using a previously described procedure, with minor modifications.[28] Chloroquine diphosphate (5.00 g, 9.69 mmol) was dissolved in 100 mL H_2O and 5 M NaOH (100 mL) was slowly added. After three successive extractions with CH_2Cl_2 (100 mL each), the organic fractions were combined and dried over $MgSO_4$. After filtration and removal of the solvent, the residue was dissolved in 20 mL of diethyl ether in order to remove any salt still present and the precipitate was filtered off. Chloroquine free base was obtained as a white crystalline solid after evaporation of the solvent on the vacuum pump (2.75 g, 8.59 mmol, yield = 89%).

^{1}H NMR (300 MHz, $CDCl_3$) δ 8.50 (1H, d, J 5.5 Hz, H-2), 7.94 (1H, d, J 2.1 Hz, H-8), 7.66 (1H, d, J 9.0 Hz, H-5), 7.33 (1H, dd, J 9.0, 2.1 Hz, H-6), 6.42 (1H, d, J 5.5 Hz, H-3), 5.24 (1H, d, J 7.0 Hz, -NH-), 3.71 (1H, m, H-9), 2.52 (4H, q, J 7.2 Hz, H14), 2.44 (2H, t, J 7.0 Hz, H-13), 1.62 (4H, m, H-11 and H-12), 1.31 (3H, d, J 6.0 Hz, H-10), 1.00 (6H, t, J 7.2 Hz, H-15).

5.1.3. 2,2,2-Trichloroethyl (4-((7-chloroquinolin-4-yl)amino)pentyl)(ethyl)carbamate (GG2) and 7-chloro-4-(2-methylpyrrolidin-1-yl)quinoline (GG2')

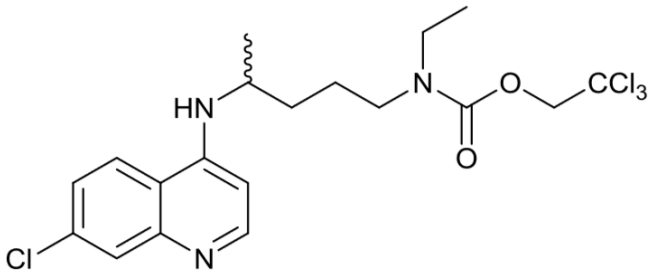

GG2

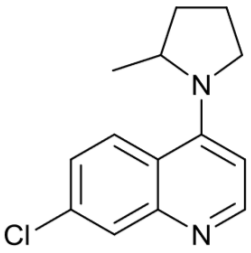

GG2'

A previously reported procedure was followed with slight modifications.[27] To a solution of chloroquine free base (220 mg, 16.32 mmol, 1 eq), in anhydrous THF (70 mL) under Ar, was added NaH (60% oil dispersion, 980 mg, 24.48 mmol, 1.5 eq) at room temperature. The solution was heated to 70°C and refluxed for three hours. The resulting cloudy yellow mixture was then cooled to room temperature and 2,2,2-trichchoroethyl chloroformate (3.37 mL, 24.48 mmol, 1.5 eq) was added dropwise. The mixture was stirred for 30 minutes at room temperature and then refluxed for 18 hours, during which time it turned brown. After cooling, the reaction was quenched with H_2O dropwise. THF was removed and the residue was treated with additional H_2O (80 mL) and extracted with diethyl ether (2 x 80 mL) and ethyl acetate (1 x 80 mL). Combined extracts were washed with brine, dried (Na_2SO_4), filtered and the solvent reduced. Column chromatography (0-100% EtOAc-hexane) gave a mixture of the chloroformate (GG2) and pyrrolidine (GG2') as a yellow gum (3.042 g); the co-products could not be separated.

5.1.4. N^4-(7-chloroquinolin-4-yl)-N^1-ethylpentane-1,4-diamine, (desethylchloroquine) (GG3)

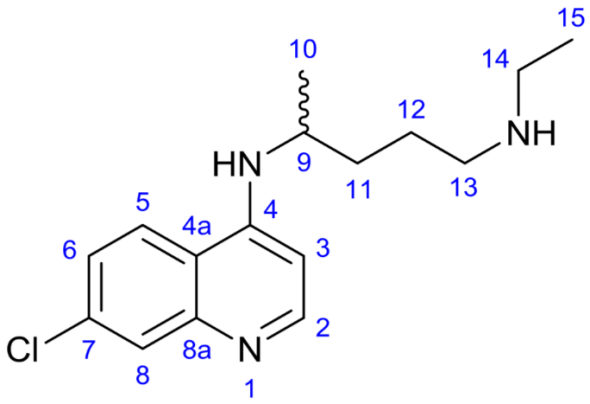

A previously reported procedure was followed with slight modifications.[27] To a flask containing a mixture of GG2 and GG2' (overall mass 3.042 g) was added a small volume of CH_2Cl_2 to dissolve the starting material and then glacial acetic acid (22 mL). Zinc dust (4.8 g, 73.44 mmol) was added in small portions and the mixture was stirred at room temperature overnight. The mixture was filtered through Celite and was subsequently washed with hot MeOH. The volume was reduced and cold 5 M NaOH was added until pH 13-14 was reached. The mixture was extracted with CH_2Cl_2 (3 x 100 mL) and the combined extracts were dried (Na_2SO_4), filtered and the solvent eliminated under vacuum The residue was dissolved in a minimum amount of CH_2Cl_2, and purified by column chromatography using 10-30% MeOH:CH_2Cl_2 followed by increasing additions of Et_3N 4% to the 35-40% MeOH:CH_2Cl_2 mobile phase for the complete elution of the product. The removal of solvent yielded GG3 as a sticky yellow-brown gum (946 mg, 3.25 mmol, yield = 20% over two steps).

^{1}H NMR (300 MHz, $CDCl_3$) δ 8.50 (1H, d, J 5.4 Hz, H-2), 7.93 (1H, d, J 2.1 Hz, H-8), 7.77 (1H, d, J 8.9 Hz, H-5), 7.33 (1H, dd, J 8.9, 2.1 Hz, H-6), 6.39 (1H, d, J 5.4 Hz, H-3), 5.59 (1H, br s, -NH-), 3.70 (1H, br s, -NH-), 3.51 (1H, m, H-9), 2.68 (4H, m, H-13 and H-14), 1.80 (1H, m, H11a), 1.70 (3H, m, H-11b and H-12), 1.31 (3H, d, J 6.3 Hz, H-10), 1.16 (3H, t, J 7.1 Hz, H-15).

5.1.5. tert-Butyl (2-((4-((7-chloroquinolin-4-yl)amino)pentyl)(ethyl)amino)ethyl)carbamate (GG4)

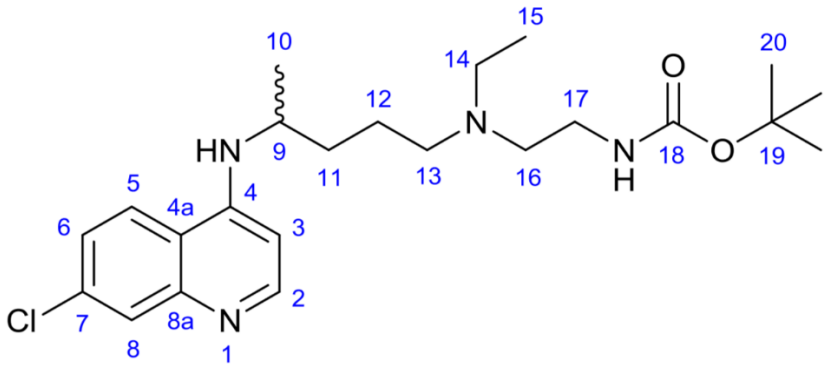

A previously reported procedure was followed with slight modifications.[38] To a flask containing desethylchloroquine (946 mg, 3.25 mmol) and N-Boc-glycinal (775 mg, 4.88 mmol) in MeOH (20 mL) was added a catalytic amount of glacial acetic acid (five drops). The reaction mixture was stirred at room temperature for 20 minutes. Thereafter, $NaBH_3CN$ (612 mg, 9.74 mmol) was added in small portions and the mixture was refluxed at 80°C for four hours. The mixture was then cooled and quenched dropwise with H_2O. The solvent was removed, NaOH 1M added until pH 12-14 was reached and the organic material extracted into CH_2Cl_2 (3 x 30 mL). The organic fractions were combined, dried (Na_2SO_4) and reduced. Column chromatography was performed with an elution gradient of 0-40% MeOH:CH_2Cl_2 to afford product GG4 (730 mg, 1.71 mmol, yield = 53%) as a light-brown oil.

^{1}H NMR (300 MHz, $CDCl_3$) δ 8.51 (1H, d, J 5.5 Hz, H-2), 7.94 (1H, d, J 2.3 Hz, H-8), 7.67 (1H, d, J 9.2 Hz, H-5), 7.34 (1H, dd, J 9.2, 2.3 Hz, H-6), 6.40 (1H, d, J 5.5 Hz, H-3), 4.90 (2H, br m, NH and carbamate -NH-) 3.71 (1H, m, H-9), 3.18 (2H, m, H-17), 2.48 (6H, m, H-13,H-14 and H-16), 1.67 (1H, m, H-11a), 1.57 (3H, m, H-11b and H-12), 1.42 (9H, s, H-20), 1.31 (3H, d, J 6.4 Hz, H-10), 0.98 (3H, t, J 6.9, H-15).

5.1.6. N^1-(2-aminoethyl)-N^4-(7-chloroquinolin-4-yl)-N^1-methylpentane-1,4-diamine (GG5)

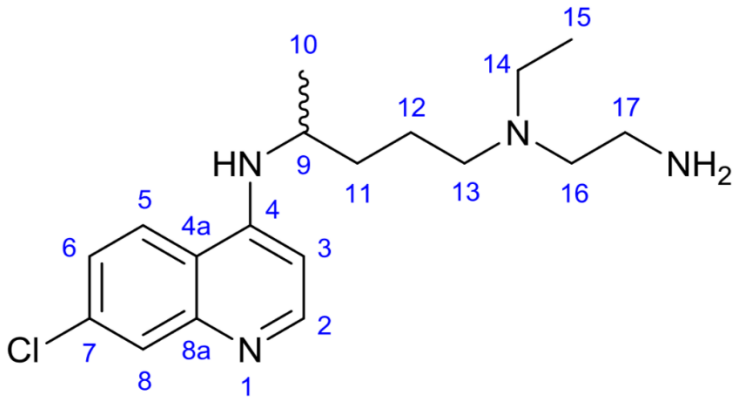

A previously reported procedure was followed with slight modifications.[38] To a stirring solution of GG4 (365 mg, 0.84 mmol, 1 eq) in 6 mL CH_2Cl_2 at 0°C was added dropwise trifluoroacetic acid (TFA, 2.1 mL, 16.82 mmol, 20 eq). The mixture was left to stir for eight hours while coming gradually to room temperature, after which TLC analysis indicated the reaction was complete. Excess solvent and TFA was removed. The residue was dissolved in 1 M NaOH (pH 14) and extracted with CH_2Cl_2 (3 x 50 mL). The organic layers were combined, dried (Na_2SO_4), filtered and reduced. The product was isolated as a light-yellow oil (231 mg, 0.69 mmol, yield = 82%), after checking purity by HPLC analysis (85%).

^{1}H NMR (400 MHz, $CDCl_3$) δ 8.48 (1H, d, *J* 5.4 Hz, H-2), 7.91 (1H, d, *J* 2.2 Hz, H-8), 7.82 (1H, d, *J* 9.0 Hz, H-5), 7.32 (1H, dd, *J* 9.0, 2.2 Hz, H-6), 6.40 (1H, d, *J* 5.4 Hz, H-3), 5.30 (1H, br s, *J* 7.2 Hz, -NH-), 3.70 (1H, m, H-9), 3.10 (2H, br s, -NH_2), 2.79 (2H, m, H-17), 2.50 (6H, m, H-13, H-14 and H-16), 1.76 (1H, m, H-11a), 1.60 (3H, m, H-11b and H-12), 1.31 (3H, d, *J* 6.4 Hz, H-10), 1.00 (3H, t, *J* 7.2, H-15).

^{13}C NMR (100 MHz, $CDCl_3$) δ 151.8 (C-2), 149.6, 149.3 (C-4, C-8a; cannot assign), 135.0 (C-7), 128.6 (C-8), 125.3 (C-6), 121.7 (C-5), 117.5 (C-4a), 99.3 (C-3), 55.2, 53.6, 47.9 (C-13, C-14, C-16; cannot assign), 48.7 (C-9), 39.4 (C-17), 34.5 (C-11), 24.2 (C-12), 20.5 (C-10), 11.7 (C-15).

5.2. Functionalization of Quantum Dots

5.2.1. General methods and instrumentation

Carboxylic acid functionalized CdSe/ZnS quantum dots (QD-COOHs) were obtained from Cytodiagnostics suspended in 1 mL deionized water (d-H_2O). In particular, previous studies[29] suggested use of QD-COOHs which present an emission peak at 630 nm due to their diameter of 6 nm in order to optimize detection during the experimental procedures.

QD-COOHs were kept refrigerated at 4°C and in the dark in order to prevent aggregation of QD-COOHs or loss of fluorescence due to exposure to natural light.

Water used in experiments was double-distilled and deionized and was provided by a Millipore Direct Q-3 water purification system.

Haem solutions were prepared daily from refrigerated haemin (Fluka®) or haematin porcine (Sigma) and kept in the dark for duration of use. All buffers were made fresh weekly and kept sealed in a Duran laboratory bottle.

A 0.01 M 4-(2-hydroxyethyl)-1 piperazineethanesulfonic acid (HEPES) (pH 7.5) buffer was made by dissolving 2.383 g HEPES in 50 mL d-H_2O and adjusting the pH with 5 M NaOH.

The pH of buffers was measured using a glass electrode and Jenway(R) 3510 pH meter calibrated with standard pH 4 and pH 7 solutions obtained from Sigma-Aldrich.

Chemicals used in all experiments were of analytical grade and obtained from Sigma-Aldrich unless otherwise stated. All glassware that came into contact with Fe(III)PPIX was acid-base washed to ensure minimal Fe(III)PPIX adsorption onto the glass. This procedure consisted in consecutive washes with: d-H_2O, 0.2 M NaOH, d-H_2O, 1 M HNO_3 and d-H_2O again. Glassware was then dried in an oven at 70 °C.

A Labnet International Inc. Prism high speed C2500-230V0 bench top microcentrifuge was used for all centrifugation of 1.5 mL Eppendorf tubes. For the washing of β-haematin in 50 mL tubes an Eppendorf 5810R centrifuge fitted with a swing rotor was used. Temperature of the centrifuge was kept constant at 21°C.

All fluorescence spectra were recorded on a Varian Carey Eclipse fluorescence spectrophotometer. A quartz fluorescence cuvette with path length of 1.5 mm and minimum readable capacity of 12 µL was used for fluorescence experiments.

A Bandelin Sonorex ultrasound bath was used for all sonication. All Fe(III)PPIX solutions were sonicated for 10 seconds prior to use.

The transmission electron microscope (TEM) used was a FEI Tecnai20 equipped with a LaB6 emitter, operating at 200 kV and fitted with a Gatan Tridiem GIF with a 2k x 2k CCD camera. Images were collected using the Digital Micrograph suite of programmes.

A Leo 1450 LaB6 scanning electron microscope with a Bruker XFlash EDS Si Drift Detector was used to obtain micrographs of prepared material. Quantification of the metal content of the quantum dots and of the elements on the surface was performed using Energy Dispersive X-ray Spectroscopy (EDS). Prior to visualization samples were sputter coated with carbon.

A Shimadzu 1800 UV-Vis series scanning spectrophotometer was used to record UV-Vis spectra over a 300 nm to 800 nm range with a medium scan rate. The temperature was kept constant at 20.0 ± 0.2 °C using a water bath. A 0.5 mL cuvette with path length of 1 cm was used.

Infrared (IR) spectra were recorded using a PerkinElmer Spectrum Two FT-IR spectrometer with a PerkinElmer UATR attachment.

Powder X-ray diffraction (PXRD) was used to confirm the structure of the bulk material. Data were collected at 298 K on a Bruker D8 Advance diffractometer with a Lynxeye detector using Cu-Kα-radiation (λ = 1.5406 Å) and operating at 40 mA and 30 kV. The sample was measured using a zero-background sample holder and was lightly ground to a fine powder before collection of data. The samples were scanned over a 2θ range of 4° to 40° using a step size of 0.02° (1760 steps) with 1.5 s exposure time.

5.2.2. Characterization of QD-COOHs

Experimental conditions and parameters of fluorescence measurements were optimised in former studies.[29]

In particular, for all excitation spectra the photomultiplier tube (PMT) voltage was set at 1000 V, to amplify the signal strength as much as possible, and the slit widths were 10 nm for excitation and 5 nm for emission. The excitation λ was set at 400 nm.

0.01 M HEPES (pH 7.5) buffer was chosen despite other buffers (PBS, TRIS) presenting a stronger signal of 630 nm QD-COOHs.

The dilution limit in d-H_2O of the sample (30 µL of the 1 mg/mL QD-COOH suspension in d-H_2O) was determined. Starting from an initial addition of 0.3 mL d-H_2O to have 1:10 QD-COOH suspension in d-H_2O and recording the fluorescence emission spectra. The level of dilution was then increased to 1:20, 1:40, 1:80 and finally 1:160 by adding d-H_2O and recording the emission spectra at each step. The PMT voltage was set at 800 V.

UV-Vis spectra of haematin were evaluated as follows: a 1.24 mM haematin stock solution was made up by dissolving 3.92 mg haematin in 5 mL 0.2 M NaOH. This stock solution (20.2 µL) was then added to 0.01 M HEPES (pH 7.5) (2.48 mL) to afford a 10 µM Fe(III)PPIX working solution. The UV-Vis absorption spectrum of the 10 µM solution was then recorded by adding 0.5 mL into the cuvette.

In order to characterize the physical size of the 630 nm QD-COOH, 30 µL of the 1 mg/mL suspension was sonicated for 2 minutes before being placed on a carbon grid and dried under a heat lamp. This sample was read directly using the TEM.

5.2.3. Derivatisation of QD-COOHs through EDC-mediated coupling

The coupling between QD-COOH and GG5 (CQ-NH_2) was achieved using 1-ethyl-3-(3-dimethylaminopropyl)carbodiimide (EDC) as coupling agent. The method reported was adapted from Kloepfer et al.[31, 32]

A 1 mM solution of GG5 was prepared by dissolving 0.34 mg of product in 1 mL 0.01 M HEPES (pH 7.5). 146 µL of this solution were added to a 1.5 mL Eppendorf tube containing 1.50 mg of EDC in 754 µL 0.01 M HEPES (pH 7.5) and vigorously shaken. 0.1 mL of unlabelled QD-COOH was then added to the reaction mixture and kept in the dark whilst stirring for 2 hours before being left overnight to ensure complete conversion. The product was washed with 0.01 M HEPES buffer (pH 7.5) and the pellet was centrifuged with the microcentrifuge at 12000 rpm for 10 minutes. In order to evaluate the presence of unreacted chloroquine derivative in the supernatant, UV-vis spectra were recorded after each washing. Once the supernatant displayed no presence of the unreacted reagent, the product was suspended in 0.3 mL of 0.01 M HEPES (pH 7.5) and stored in the dark at 4°C.

Labelled QDs (QD-CQ) were characterized by fluorescence measurements, SEM analysis with EDS-SEM and TEM microscopy.

In particular, 30 µL of the product were suspended in 0.01 M HEPES (pH 7.5), placed on a carbon grid and dried under a heat lamp. This sample was read directly using the TEM.

For SEM analysis, 30 µL of the product were suspended in 0.01 M HEPES (pH 7.5), placed on a metal stub, dried under a heat lamp and sputter coated with carbon before being analysed with scanning electron microscopy using EDS.

5.3. Interactions of Quantum Dots and Functionalized Quantum Dots

5.3.1. Behaviour of QD-CQ

In order to investigate the behaviour of QD-CQ, especially regarding their tendency to aggregate, the fluorescence emission spectra of 630 nm labelled and unlabelled QDs diluted 1:5 in 0.01 M HEPES (pH 7.5) were recorded with $\lambda_{excitation}$ = 400 nm and PMT = 1000 V. The sample was left at room temperature (20°C) for 4 hours after which the fluorescence emission spectrum was rerecorded.

The same procedure was used for other samples made using 17 µL of QD-CQ, 70 µL 0.01 M HEPES (pH 7.5) and 50 µL of another solvent (acetone, methanol, ethanol).

In addition, for both labelled and unlabelled QDs, a sample was prepared by adding 17 µL of QDs suspension and 120 µL of 0.01 M HEPES (pH 4.2), then investigated using the same method.

5.3.2. Spectrophotometric analysis of interactions of QD-COOHs and QD-CQs with CQ and Fe(III)PPIX

In order to study the interactions between quantum dots and Fe(III)PPIX, fluorescence titrations of QD-COOHs and QD-CQs were performed using both CQ and Fe(III)PPIX. Concentrations and conditions detailed below are the standard conditions that were chosen and were varied for replicates. GraphPad Prism[39] was used to analyse binding as one-site thermodynamic association for all titrations, each one performed in triplicate.

QD-COOH $\lambda_{emission}$ (nm)	PMT (V)	$\lambda_{excitation}$ (nm)	Slit Widths (nm) excitation; emission	Scan speed
630	1000	400	10; 5	slow

5.3.3. Spectrophotometric titrations of QD-COOHs

Chloroquine

A 0.5 mM CQ solution was made by dissolving 1.29 mg of chloroquine diphosphate salt (M=515.86 g/mol) in 5 mL 0.01 M HEPES (pH 7.5). This solution was used for titrating 630 nm QD-COOHs diluted in 0.01 M HEPES (pH 7.5) (1:20 dilution in 60 µL) in a cuvette. Additions were done in 3.00 µL increments. After each addition the solution was stirred and the fluorescence spectra recorded using the standard fluorimeter settings. The whole titration was performed thrice.

Fe(III)PPIX

A 0.813 mM Fe(III)PPIX stock solution was made by dissolving 1.03 mg haematin (M=633.49 g/mol) in 2 mL 0.1 M NaOH which was then further diluted to a 15.9 µM working solution in 0.01 M HEPES (pH 7.5) with total volume 1 mL. This working solution was then used for titrating 630 nm QD-COOHs diluted in 0.01 M HEPES (pH 7.5) (1:20 dilution in 30 µL) in a cuvette. Additions were done in 5.00 µL increments. After each addition the solution was stirred and the fluorescence spectra recorded using the standard fluorimeter settings. The whole titration was performed thrice. After the end of the titration, 5 µL of a solution of 0.5 mM chloroquine was added to the cuvette, mixed and the spectrum recorded.

5.3.4. Spectrophotometric titrations of QD-CQs

Chloroquine

A 0.05 mM CQ solution was made by diluting 0.5 mL of the 0.5 mM chloroquine solution previously prepared with 4.5 mL 0.01 M HEPES (pH 7.5). This solution was used for titrating 630 nm QD-COOHs diluted in 0.01 M HEPES (pH 7.5) (1:2 dilution in 30 µL) in a cuvette. Additions were done in 3.00 µL increments. After each addition the solution was stirred and the fluorescence spectra recorded using the standard fluorimeter settings. The whole titration was performed thrice.

Fe(III)PPIX

A 0.939 mM Fe(III)PPIX stock solution was made by dissolving 1.19 mg haematin (M=633.49 g/mol) in 2 mL 0.1 M NaOH which was then further diluted to a 37.57 µM working solution in 0.01 M HEPES (pH 7.5) with total volume 1 mL. This working solution was then used for titrating 630 nm QD-CQs

diluted in 0.01 M HEPES (pH 7.5) (1:2 dilution in 30 µL) in a cuvette. Additions were done in 3.00 µL increments. After each addition the solution was stirred and the fluorescence spectra recorded with PMT = 1000 V and $\lambda_{excitation}$ = 420 nm, considered optimal to avoid the absorption of the light by Fe(III)PPIX in solution. After the end of the titration, 5 µL of a solution of 0.5 mM chloroquine was added to the cuvette, mixed and the spectrum recorded.

5.3.5. Synthesis of β-Haematin[35]

A 9.7 M sodium acetate buffer was made in accordance with the Henderson-Hasselbalch equation by adding 23.76 g sodium acetate trihydrate to 20 mL d-H_2O and 17.81 mL acetic acid with stirring. The pH was adjusted to 4.8 using 5 M NaOH. A 9.25 mM haemin solution was made by dissolving 30.17 mg haemin (M=651.94 g/mol) in 5 mL 0.1 M NaOH. Two glass vessels were set up with stirrer bars and a water bath set to 60°C. To both vessels was added 2.5 mL haemin solution, 250 µL 1M HCl and 2.31 mL sodium acetate buffer (9.7 M) while stirring. One vessel was quenched immediately with excess d-H_2O. Both vessels were then covered with watch glasses and incubated for 1 hour before being quenched with d-H_2O and placed on ice. Products were washed with d-H_2O and suction filtered through a nitrocellulose filter (pore size 0.22 µM). A 5 % pyridine washing solution was then made from 0.25 mL pyridine, 2 mL acetone, 1 mL 0.01 M HEPES (pH 7.5) and 1.75 mL d-H_2O. The products were dried in the oven until the surface cracked and then placed in 1.5 mL Eppendorf tubes. Five subsequent washings were then done with d-H_2O which involved microcentrifugation for 10 mins at 10000 rpm between each washing. Product formation was confirmed with FTIR and PXRD.[35]

5.3.6. Transmission electron microscopy analysis of interactions of QD-COOH and QD-CQs with β-haematin

To 30 µL of the 630 nm QD-CQs suspension 0.12 mg of β-haematin was added. The sample was vortexed briefly before being placed on a carbon grid and dried under a heat lamp. This sample was visualised directly using the TEM. The same procedure was repeated for a sample of QD-COOHs prepared by adding 10 µL of the unlabelled nanoparticles in d-H_2O suspension to 20 µL of 0.01 M HEPES (pH 7.5).

CHAPTER 6

REFERENCES

1 WHO, *World Malaria Report 2017*, WHO, 29 November 2017.

2 WHO, *Malaria Fact Sheet N°94,* WHO, March 2014.

3 Murray CJ, Rosenfeld LC, Lim SS, Andrews KG, Foreman KJ, Haring D, Fullman N, Naghavi M, Lozano R, Lopez AD, Lancet, 2012, 379 (9814): 413–31.

4 WHO, *World Malaria Report 2014*, WHO, 2014.

5 WHO, *World Malaria Report 2015*, WHO, 2015.

6 S. Riaz, *Malaria and Plasmodium*, 1, http://www.slideshare.net, March 2012.

7 P. A. Sigala and D. E. Goldberg, Annu. Rev. Microbiol., 2014, 68, 259.

8 T. J. Egan, Mol. Biochem. Parasitol., 2008, 157, 127-136 (DOI:10.1016/j.molbiopara.2007.11.005).)

9 S. Pagola, P. W. Stephens, D. S. Bohle, A. D. Kosar and S. K. Madsen, Nature (London), 2000, 404, 307-310, (DOI: 10.1038/35005132).

10 J. Woodland, *PHD Thesis*, UCT, August 2016.

11 C. D. Fitch, R. Chevli, H. S. Banyal, G. Phillips, M. A. Pfaller and D. J. Krogstad, Antimicrob. Agents Chemother., 1982, 21, 819.

12 A. C. Chou and C. D. Fitch, J. Clin. Invest., 1980, 66, 856.

13 J. M. Combrinck, T. E. Mabotha, K. K. Ncokazi, M. A. Ambele, D. Taylor, P. J. Smith, H. C. Hoppe and T. J. Egan, ACS Chem. Biol., 2013, 8, 133.

14 Jill M. Combrinck, Kim Y. Fong, Liezl Gibhard, Peter J. Smith, David W. Wright and Timothy J. Egan, Malaria Journal, 2015, 14, 253.

15 R. Buller, M. L. Peterson, O. Almarsson and L. Leiserowitz, Crystal Growth & Design, 2002, 2 (DOI:10.1021/cg025550i).

16 I. Weissbuch and L. Leiserowitz, Chem. Rev. (Washington, DC, U. S.), 2008, 108, 4899-4914 (DOI:10.1021/cr078274t).

17 I. Solomonov, M. Osipova, Y. Feldman, C. Baehtz, K. Kjaer, I. K. Robinson, G. T. Webster, D. McNaughton, B. R. Wood, I. Weissbuch and L. Leiserowitz, Leslie, Journal of the American Chemical Society, 2007, 129, 2615-27 (DOI:10.1021/ja0674183).

18 K. N. Olafson, M. A. Ketchum, J. D. Rimer and P. G. Vekilov, Proc. Natl. Acad. Sci. USA, 2015, 112, 4946.

19 J. Lakowicz, *Principles of Fluorescence Spectroscopy*, Springer, Baltimore, Maryland, USA, 2006.

20 U. Resch-Genger, M. Grabolle, S. Cavaliere-Jaricot, R. Nitschke and T. Nann, Nat. Methods, 2008, 5, 763-775 (DOI:10.1038/nmeth.1248).

21 S. Mazumder, R. Dey, M. K. Mitra, S. Mukherjee and G. C. Das, J. Nanomater., 2009, (DOI:10.1155/2009/815734).

22 I. L. Medintz, H. T. Uyeda, E. R. Goldman and H. Mattoussi, Nat. Mater., 2005, 4, 435-446 (DOI:10.1038/nmat1390).

23 B. O. Dabbousi, J. Rodriguez-Viejo, F. V. Mikulec, J. R. Heine, H. Mattoussi, R. Ober, K. F. Jensen and M. G. Bawendi, J Phys Chem B, 1997, 101, 9463-9475 (DOI:10.1021/JP971091Y).

24 Cytodiagnostics, Product Data Sheet - TriliteTM Fluorescent Nanocrystals 490nm - Carboxy, www.cytodiagnostics.com.

25 Inivitrogen, *Qdot® ITK™ Carboxyl Quantum Dots Experimental Protocol*, Molecular Probes Inc., 2007.

26 W. R. Algar, M. H. Stewart, A. M. Scott, W. J. Moon and I. L. Medintz, J. Mater. Chem. B, 2014, 2, 7816-7827 (DOI:10.1039/C4TB00985A).

27 M. Ansari and J. C. Craig, Synthesis, 1995, 147.

28 W. I. Sundquist, D. P. Bancroft and J. Lippard, J. Am. Chem. Soc., 1990, 112, 1590.

29 H. Knight, *Honours Project*, UCT, November 2016.

30 A. F. G. Slater, W. J. Swiggard, B. R. Orton, W. D. Flitter, D. E. Goldberg, A. Cerami and G. B. Henderson, Proc. Natl. Acad. Sci. U. S. A., 1991, 88, 325-9 (DOI:10.1073/pnas.88.2.325).

31 J. A. Kloepfer, R. E. Mielke and J. L. Nadeau, Appl. Environ. Microbiol., 2005, 71, 2548-2557 (DOI:10.1128/AEM.71.5.2548-2557.2005).

32 J. A. Kloepfer, R. E. Mielke, M. S. Wong, K. H. Nealson, G. Stucky and J. L. Nadeau, Appl. Environ. Microbiol., 2003, 69, 4205-4213 (DOI:10.1128/AEM.69.7.4205-4213.2003).

33 Timothy J. Egan, Roger Hunter, Catherine H. Kaschula, Helder M. Marques, Ashley Misplon and Jason Walden, Journal of Medicinal Chemistry, 2000, 43 (2), 283-291 (DOI: 10.1021/jm990437l).

34 T. J. Egan, J. M. Combrinck, J. Egan, G. R. Hearne, H. M. Marques, S. Ntenteni, B. T. Sewell, P. J. Smith, D. Taylor, S. D. A. van and J. C. Walden, Biochem. J., 2002, 365, 343-7, (DOI: 10.1021/cb300454t).

35 J. Gildenhuys, T. l. Roex, T. J. Egan and K. A. deVilliers, J. Am. Chem. Soc., 2013, 135, 1037-1047 (DOI:10.1021/ja308741e).

36 D. S. Bohle, R. E. Dinnebier, S. K. Madsen and P. W. Stephens, J. Biol. Chem., 1997, 272, 713-716 (DOI:10.1074/jbc.272.2.713).

37 X. Michalet, F. F. Pinaud, L. A. Bentolila, J. M. Tsay, S. Doose, J. J. Li, G. Sundaresan, A. M. Wu, S. S. Gambhir and S. Weiss, Science (Washington, DC, U. S.), 2005, 307, 538-544 (DOI:10.1126/science.1104274).

38 M. Cabrera, J. Natarajan, M. Paguio, C. Wolf, J. Urbach and P. D. Roepe, Biochemistry, 2009, 48, 9471.

39 GraphPad Software Inc., GraphPad Prism, 10855 Sorrento Valley Rd. #203, San Diego. CA 92121., 2008.